TECTONICS, VOL. 33, 1–21, doi:10.1002/2013TC003398, 2014

Multiple migmatite events and cooling from granulite facies metamorphism within the Famatina arc margin of northwest Argentina

Sean R. Mulcahy,[1] Sarah M. Roeske,[2] William C. McClelland,[3] Joshua R. Ellis,[4] Fred Jourdan,[5] Paul R. Renne,[1,6] Jeffrey D. Vervoort,[7] and Graciela I. Vujovich[8]

Received 18 June 2013; revised 14 October 2013; accepted 19 November 2013.

[1] The Famatina margin records an orogenic cycle of convergence, metamorphism, magmatism, and extension related to the accretion of the allochthonous Precordillera terrane. New structural, petrologic, and geochronologic data from the Loma de Las Chacras region demonstrate two distinct episodes of lower crustal migmatization. The first event preserves a counterclockwise pressure-temperature path in kyanite-K-feldspar pelitic migmatites that resulted in lower crustal migmatization via muscovite dehydration melting at ∼12 kbar and 868°C at 461 ± 1.7 Ma. The shape of the pressure temperature path and timing of metamorphism are similar to those of regional midcrustal granulites and suggest pervasive Ordovician migmatization throughout the Famatina margin. One-dimensional thermal modeling coupled with regional isotopic data suggests Ordovician melts remained at temperatures above their solidus for 20–30 Ma following peak granulite facies metamorphism, throughout a time period marked by regional oblique convergence. The onset of synconvergent extension occurred only after regional migmatites cooled beneath their solidus and was synchronous with the cessation of Precordillera terrane accretion at ∼436 Ma. The second migmatite event was regionally localized and occurred at ∼700°C and 12 kbar between 411 and 407 Ma via vapor saturated melting of muscovite. Migmatization was synchronous with extension, exhumation, and strike-slip deformation that likely resulted from a change in the plate boundary configuration related to the convergence and collision of the Chilenia terrane.

Citation: Mulcahy, S. R., S. M. Roeske, W. C. McClelland, J. R. Ellis, F. Jourdan, P. R. Renne, J. D. Vervoort, and G. I. Vujovich (2014), Multiple migmatite events and cooling from granulite facies metamorphism within the Famatina arc margin of northwest Argentina, *Tectonics*, *33*, doi:10.1002/2013TC003398.

1. Introduction

[2] Transitions from convergence to extension during an orogenic cycle result from the linked interaction between plate bounding forces, the thermal and rheologic evolution of the lithosphere, and contrasts in gravitational potential energy within an orogen [e.g., *England and Thompson*, 1986; *Dewey*, 1988]. The presence of melt in the middle and lower crust, in particular, exerts a profound effect on the rheology of orogenic belts and in facilitating a change from convergence to extension and orogenic collapse [e.g., *Vanderhaeghe and Teyssier*, 1997; *Teyssier and Whitney*, 2002]. Determining whether or not melting was an effective driving mechanism of extension within a given orogen requires accurately constraining the timing and duration of melting events in the crust with respect to plate convergence, terrane accretion, lithospheric extension, and exhumation.

[3] The Sierras Pampeanas of northwest Argentina (Figure 1) record the evolution of a Cambrian convergent margin to an Ordovician collisional orogen that experienced middle-to-lower crustal granulite facies metamorphism [e.g., *Otamendi et al.*, 2008, and references therein] and Silurian synconvergent extension [*Mulcahy et al.*, 2011]. Regional convergence associated with Famatina arc magmatism initiated as a result of east dipping subduction as early as ∼515–495 Ma, although the majority of arc magmatism occurred from ∼485 to 465 Ma [*Pankhurst and Rapela*,

Additional supporting information may be found in the online version of this article.

[1]Department of Earth and Planetary Science, University of California, Berkeley, California, USA.
[2]Department of Geology, University of California, Davis, California, USA.
[3]Department of Geoscience, University of Iowa, Iowa City, Iowa, USA.
[4]Kinross Gold Corporation, Toronto, Ontario, Canada.
[5]Western Australian Argon Isotope Facility, Department of Applied Geology and JdLCMS, Curtin University, Perth, Western Australia, Australia.
[6]Berkeley Geochronology Center, Berkeley, California, USA.
[7]School of Earth and Environmental Sciences, Washington State University, Pullman, Washington, USA.
[8]Department of Geology, University of Buenos Aires-CONICET, Buenos Aires, Argentina.

Corresponding author: S. R. Mulcahy, Department of Earth and Planetary Science, University of California, 307 McCone Hall, Berkeley, CA 94720-4767, USA. (mulcahy@berkeley.edu)

0278-7407/14/10.1002/2013TC003398

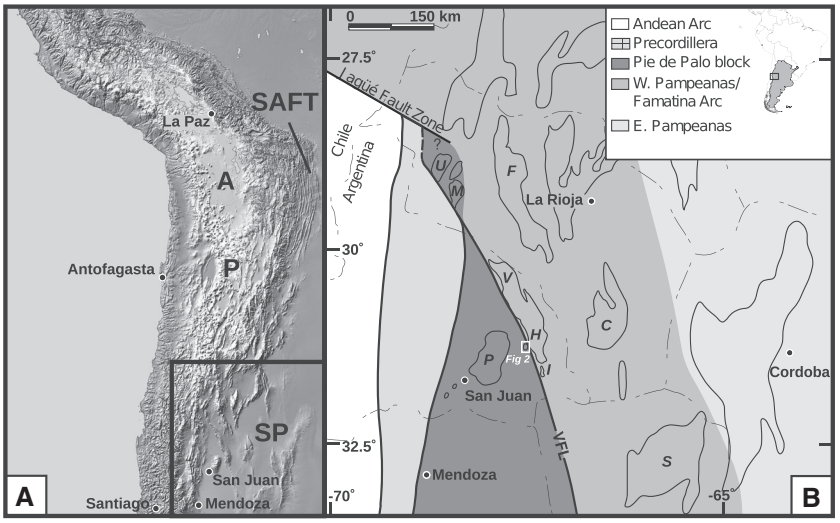

Figure 1. (a) Shaded relief map of western South America illustrating the geographic location of the study area within the Sierras Pampeanas (SP). Geologic provinces labeled for reference are the Altiplano (A) and Puna plateau (P) and the Southern Andean fold and thrust belt (SAFT). (b) Tectonic map of northwest Argentina. Thick lines mark intraterrane boundaries, and thin dash-dotted lines mark country and province boundaries. Individual ranges shown for reference are F, Sierras de Famatina; H, Sierras de la Huerta; LLC, Loma de Las Chacras; M, Sierras de Maz; P, Sierras de Pie de Palo; S, Sierras de San Luis; U, Sierra de Umango; and V, Valle Fertil.

1998; *Pankhurst et al.*, 2000; *Quenardelle and Ramos*, 1999; *Mulcahy et al.*, 2007; *Ducea et al.*, 2010]. Stratigraphic evidence within the Precordillera terrane [*Astini et al.*, 1995; *Astini*, 1998; *Thomas and Astini*, 2007] and top-to-the-west ductile shear zones with the Sierra de Pie de Palo [*Mulcahy et al.*, 2011] suggest that initial collision of the Precordillera with the Famatina arc margin began by ∼470 Ma and that the terrane had fully collided by the Late Ordovician (∼458–449 Ma). Top-to-the-east ductile shear zones within the Sierra de Pie de Palo (Figure 1) suggest synconvergent extension initiated at middle-to-lower crustal depths at ∼436 Ma with continued extension and exhumation ∼417 Ma [*Mulcahy et al.*, 2011].

[4] Peak granulite facies metamorphism is spatially associated with the Famatina arc, but different crustal levels are exposed on either side of the Valle Fertil lineament. Andalusite and sillimanite bearing pelitic protoliths east of the Valle Fertil Lineament experienced migmatization (Figure 1) at ∼750–900°C at ∼5–7 kbar via the intrusion of mafic and intermediate melts during construction of the Famatina arc [e.g., *Hauzenberger et al.*, 2001; *Büttner et al.*, 2005; *Murra and Baldo*, 2006; *Delpino et al.*, 2007; *Castro de Machuca et al.*, 2008; *Otamendi et al.*, 2008; *Gallien et al.*, 2010; *Tibaldi et al.*, 2011; *Larrovere et al.*, 2011; *Otamendi et al.*, 2012; *Tibaldi et al.*, 2013] and preserve counterclockwise pressure-temperature paths and near isobaric cooling from peak temperatures [e.g., *Hauzenberger et al.*, 2001; *Delpino et al.*, 2007; *Otamendi et al.*, 2008; *Gallien et al.*, 2010]. Migmatization occurred at ∼465 Ma, although ages from multiple systems within the high-grade rocks range from ∼470 to 402 Ma [e.g., *Hauzenberger et al.*, 2001; *Hockenreiner et al.*, 2003; *Lucassen and Becchio*, 2003; *Galindo et al.*, 2004; *Porcher et al.*, 2004; *Büttner et al.*, 2005; *Steenken et al.*, 2006; *Castro de Machuca et al.*, 2008; *Steenken et al.*, 2008; *Gallien et al.*, 2010; *Varela et al.*, 2011] and have been interpreted as cooling from peak conditions or as distinct metamorphic and deformation events. West of the Valle Fertil lineament, kyanite-K-feldspar granulite facies rocks of the Loma de Las Chacras (Figures 1) experienced lower crustal migmatization at ∼750–800°C at ∼11–12 kbar at ∼465 Ma [*Baldo et al.*, 2001; *Casquet et al.*, 2012].

[5] While the timing of regional melting is well documented in relation to regional convergence, terrane accretion, and extension, the number, duration, and extent of melting episodes with respect to these events is poorly constrained. We combine structural mapping, thermobarometry, and geochronology using multiple isotopic systems to constrain the deformation, metamorphic, and magmatic history of the Loma de Las Chacras region. The data define two distinct episodes of migmatization. Ordovician granulite facies migmatization was synchronous with accretion of the Precordillera terrane and predated synconvergent extension. Devonian migmatization was regionally localized and is associated with the formation of a new plate margin. Synconvergent extension within the Famatina margin was not contemporaneous with either melting event and is more likely related to changes in plate boundary forces following terrane accretion.

2. Geology of the Loma de Las Chacras

[6] The Loma de Las Chacras (herein referred to as Las Chacras) is located along the western margin of the Sierra de la Huerta (Figures 1 and 2). *Vujovich* [1994] first described the geology and petrology of the region and interpreted Las Chacras to represent the amphibolite facies, igneous-

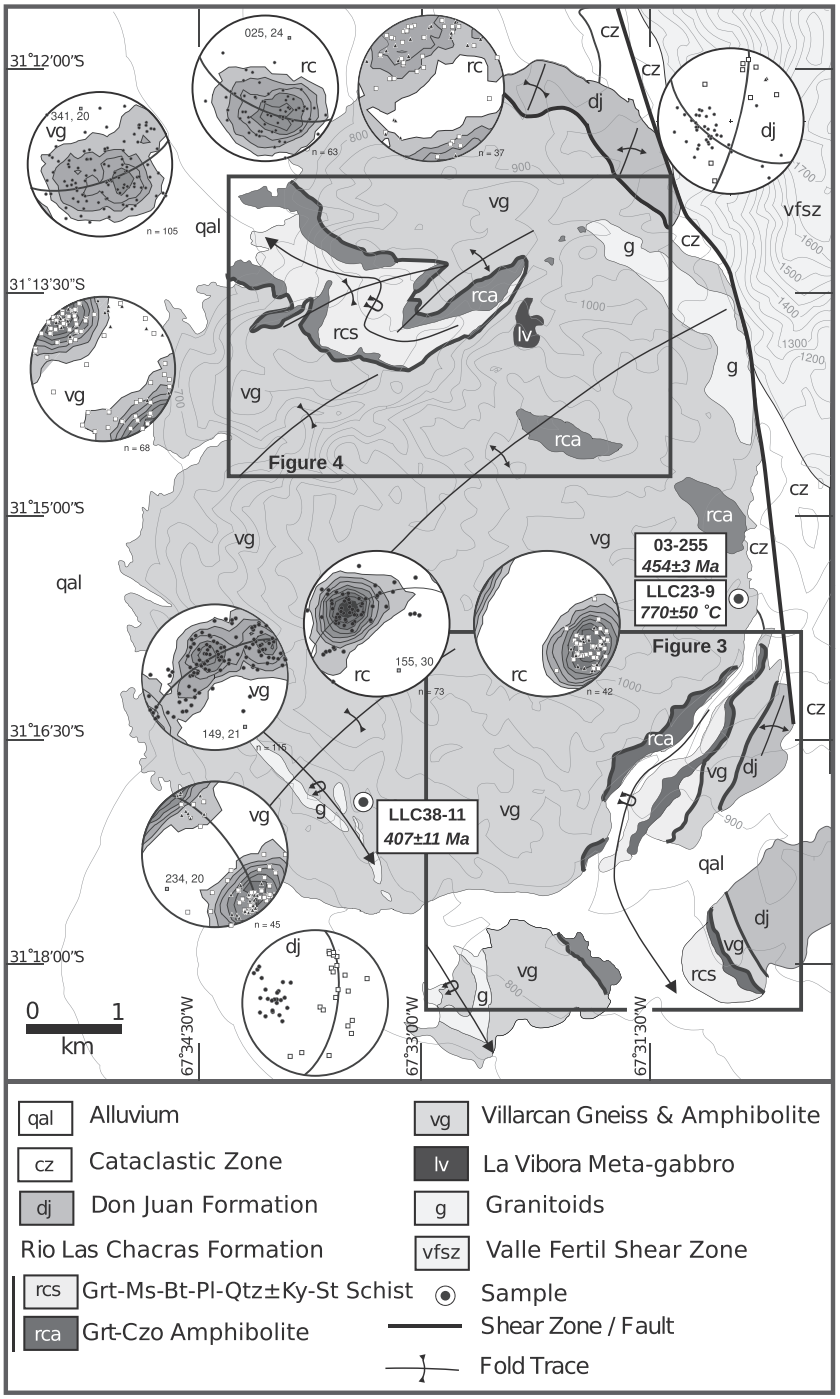

Figure 2. Geologic map of the Loma de Las Chacras displaying the first order structures. The locations of more detailed geologic maps are outlined in the black rectangles, and the locations and results of samples studied for thermobarometry and geochronology are shown with circles with sample numbers and data given in the adjacent boxes.

metamorphic basement to the Sierra de la Huerta. The region consists of mafic and ultramafic intrusive rocks, intermediate orthogneiss and leucocratic bodies, pelitic migmatites, amphibolites, and pelitic schists [*Vujovich*, 1994]. Previous workers estimated migmatization occurred at ∼12 kbar and ∼780°C and zircon U-Pb ages from migmatitic leucosome record melting a ∼468 Ma [*Baldo et al.*, 2001; *Casquet et al.*, 2012]. In what follows, we first summarize the tectonostratigraphy of Las Chacras and then discuss the structural and metamorphic evolution of the region.

2.1. Lithologic Units

[7] We recognize four distinct units, modified from *Vujovich* [1994], based on protolith, mineral assemblage, and metamorphic grade (Figure 2). From high to low structural levels the units are the Don Juan Formation, the Rio

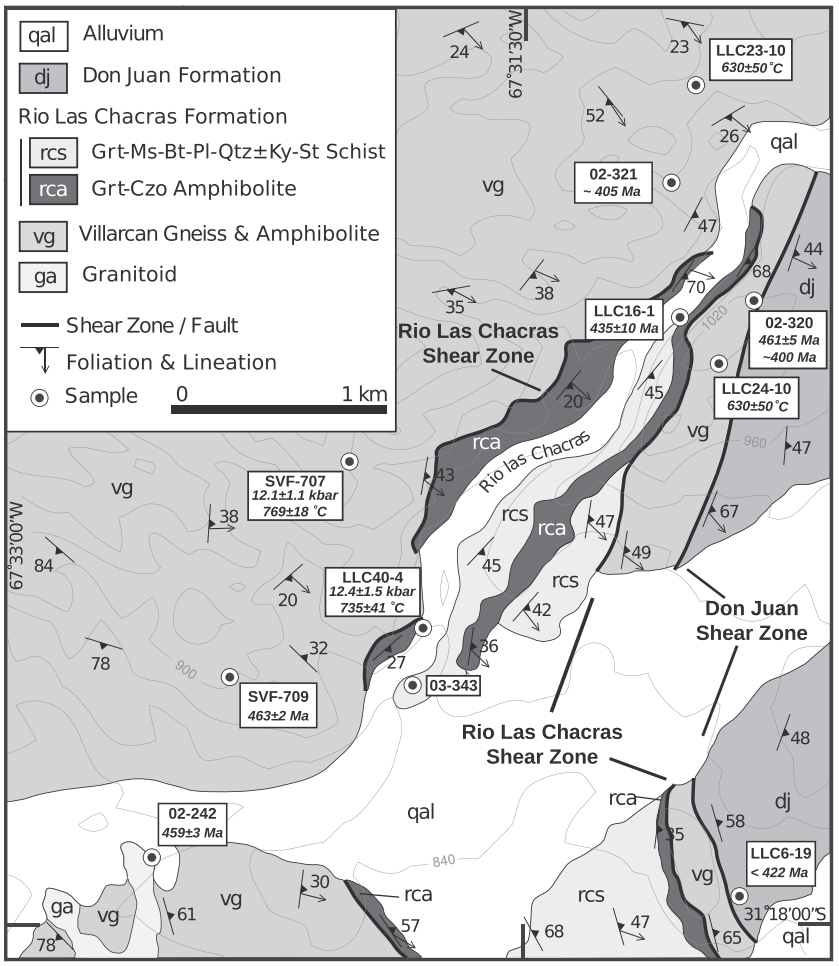

Figure 3. Geologic map of the southern portion of the Loma de Las Chacras. Sample locations dated by various isotopic systems and their ages, as well as samples used for thermobaromtery, as well as inset stereoplots of structural elements are shown. See text for discussion. Sample SV-707 and SV-709 are approximately located from [*Baldo et al.*, 2001].

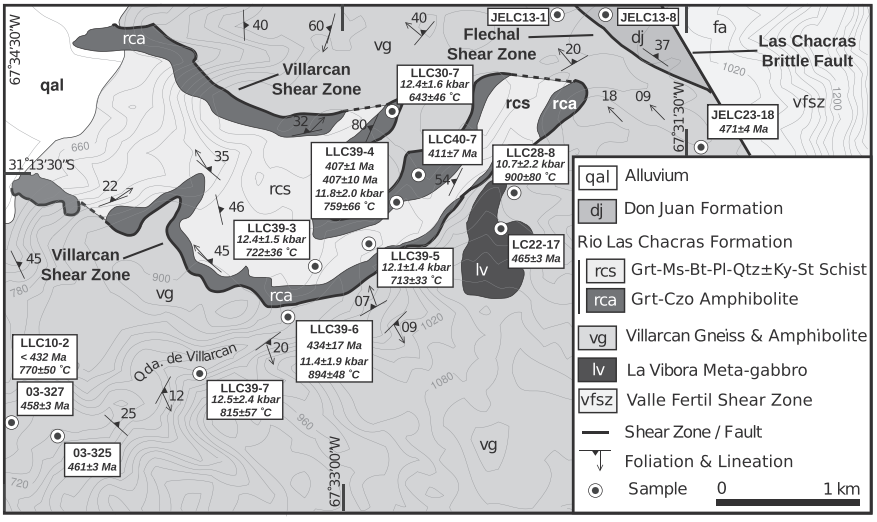

Figure 4. Geologicmap of the northern portion of the Loma de Las Chacras. Sample locations dated by various isotopic systems and their ages, as well as samples used for thermobaromtery, as well as inset stereoplots of structural elements are shown. See text for discussion.

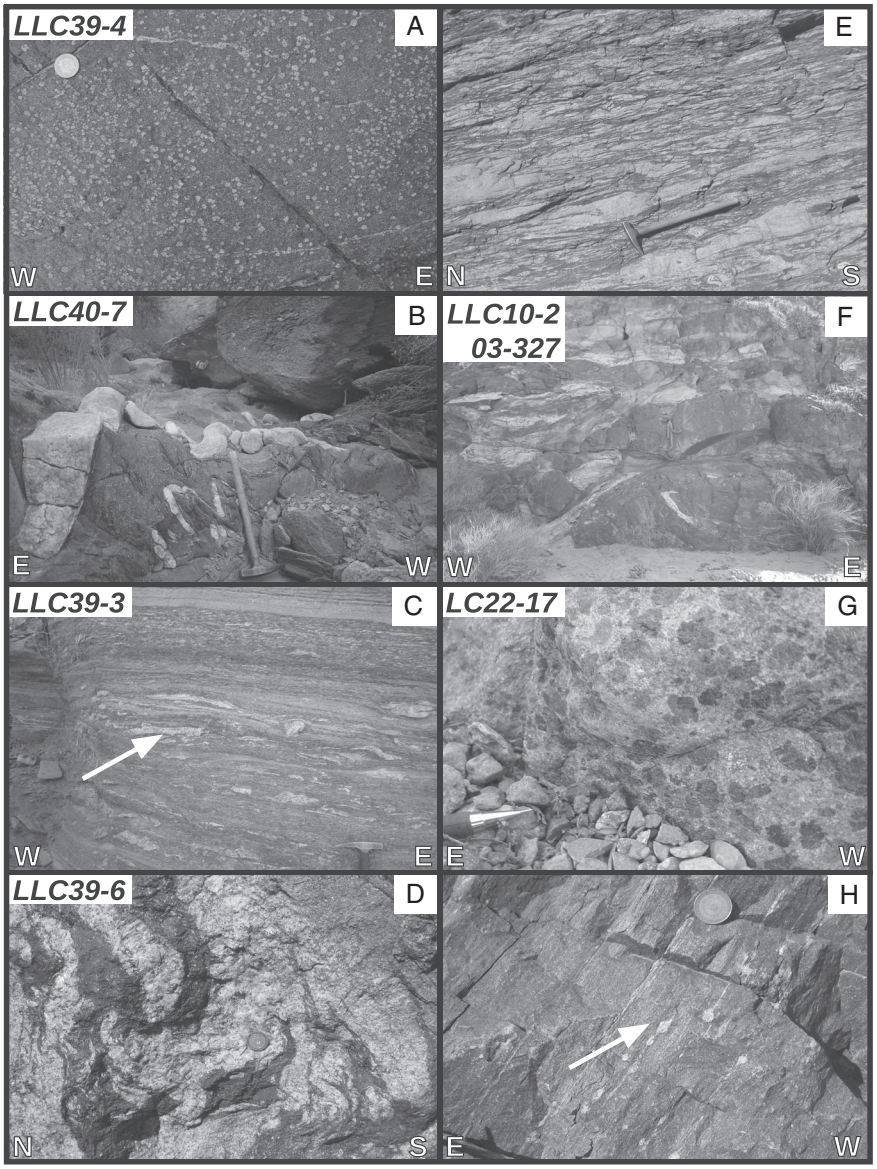

Figure 5. Outcrop photographs from the Loma de La Chacras. Images with sample numbers refer to specific locals shown on the maps and discussed in the text. (a) Grt-Czo amphibolite of the Rio las Chacras Formation from Quebrada Villarcan. (b) Igneous body intruding the Rio las Chacras amphibolite, folded by F_B. (c) Compositional banding within schist of the Rio las Chacras Formation. The arrow points to low-volume, foliation-parallel leucosome. Hammer head for scale. (d) Stromatitic migmatite of the Villarcan Gneiss, Argentine peso for scale. (e) Deformed migmatite of the Villarcan Gneiss immediately beneath the Villarcan shear zone. (f) Amphibolite body within the Villarcan Gneiss with interlayered trondhjemite sills. (g) Coarse amphibole as a pseudomorph for pyroxene within the La Vibora metagabbro. (h) Mylonitic fabric of the Flechal shear zone developed within the Villarcan Gneiss, the arrow points to plagioclase sigma-clast indicating top-to-the-east sense of motion.

Las Chacras Formation, the Villarcan Gneiss, and the La Vibora formation.

[8] The Don Juan Formation occurs in the southeast and northeast margins of Las Chacras (Figure 2) and is separated from underlying units by the Don Juan shear zone in the south (Figure 3) [*Cain*, 2006] and the Flechal shear zone in the north (Figure 4). The unit predominantly consists of quartzite and pelitic Qtz-Ms-Bt-Chl schist (mineral abbreviations after *Kretz* [1983]). Lesser amounts of Cal-Qtz-Ms marble and Amp-Ep/Czo-Plg-Qtz amphibolite also occur within the formation.

[9] The Rio Las Chacras Formation is best exposed in the Rio Las Chacras and Quebrada Villarcan (Figure 2). The formation consists of Grt-Czo amphibolite and pelitic schist. The two lithologies are structurally concordant, and the schist is structurally higher than the amphibolite. The formation is separated from the overlying Don Juan Formation by the Don Juan and Flechal shear zones and from the

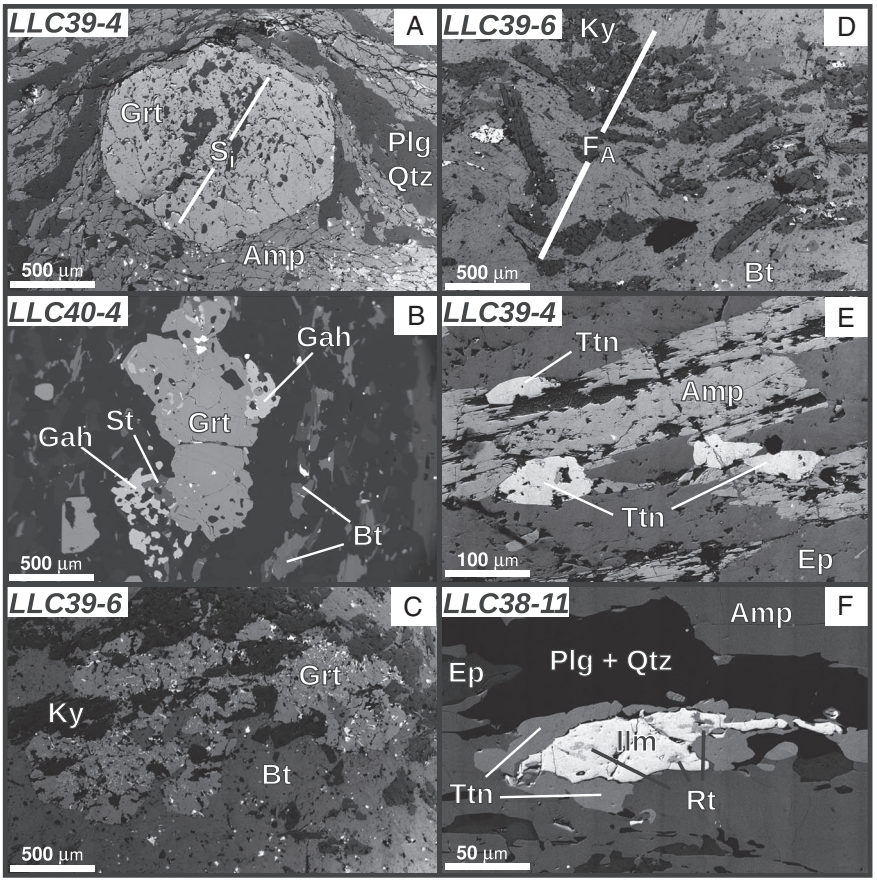

Figure 6. Backscattered electron images of samples from the Loma de Las Chacras. (a) Poikilitic garnet within the Rio Las Chacras amphibolite showing internal fabric at a high angle to the surrounding external foliation. (b) Rio Las Chacras schist containing the assemblage Grt-Bt-Ms-Qtz-Plg-St-Gah. (c) Garnet within migmatite of the Villarcan Gneiss with inclusions of Ky and Bt. (d) Melanosome of the Villarcan Gneiss folded by F_A. (e) Titanite aligned within the foliation of Rio Las Chacras amphibolite. (f) Titanite surrounding ilmenite containing rutile inclusions in amphibolite of the Villarcan Gneiss.

underlying Villarcan Gneiss by the Rio Las Chacras shear zone (Figure 3) and Villarcan shear zone (Figure 4). The amphibolite contains the assemblage Amp-Grt-Czo-Pl-Qtz-Ttn ± Rt (Figure 5a) and forms laterally continuous horizons up to ∼70 m thick that define much of the structure within the southern (Figure 3) and northern (Figure 4) portions of the range. The amphibolite is locally intruded by melts of intermediate composition (Figure 5b). The unit displays a foliation defined by amphibole, plagioclase, and clinozoisite (Figure 6a) and is deformed by second-generation folds (Figure 4). The mineral lineation is defined by aligned amphibole and clinozoisite. The Rio Las Chacras schist contains alternating bands of metapelite and metagreywacke (Figure 5c) that contain the assemblage Ms-Bt-Grt-Plg-Qtz ± Ky, with less common staurolite and gahnite (Figure 6b). The unit contains ≤ 10% leucocratic melt, which is largely concordant with foliation in the schist. The lineation is defined by aligned muscovite and biotite.

[10] The Villarcan Gneiss occupies the lowest structural level and constitutes the majority of the outcrops within Las Chacras [*Vujovich*, 1994]. The unit consists of variably deformed pelitic migmatite, amphibolite, orthogneiss, and tonalite. The migmatites are stromatitic at low structural levels (Figure 5d) but become progressively more foliated approaching the Villarcan and Rio las Chacras shear zones (Figure 5e). Melanosome within the migmatite contains the assemblage Grt-Ky-Kfs-Plg-Bt-Op ± Ms ± Qtz (Figure 6c). Aligned biotite, kyanite, and opaque minerals define the foliation in the melanosome (Figure 6d), and quartz is commonly absent. The leucosome contains the assemblage Plg-Kfs-Qtz ± Ky. Amphibolites are common within the Villarcan Gneiss and occur as thin (submeter scale) concordant bodies or as larger (meter scale) asymmetric bodies around which the migmatitic gneiss is strained (Figure 5f). The amphibolites largely lack garnet and contain the assemblage Amp-Czo-Plg-Qtz-Ttn ± Bt. Foliation is defined by aligned amphibole plagioclase, and quartz and a mineral lineation is defined by aligned amphibole and clinozoisite.

[11] The La Vibora formation consists of small (meter scale) outcrops of coarse-grained metahornblendite [*Vujovich*, 1994] that are interpreted as a metamorphosed gabbro/pyroxenite (Figure 5g). The unit contains the assemblage Amp-Czo-Plg-Qtz-Bt-Ttn ± En-Di. Hornblende forms pseudomorphs of large (0.5–1.5 cm) and randomly aligned pyroxene [*Vujovich*, 1994]. Variably deformed and metamorphosed outcrops can be found throughout the Villarcan Gneiss where both units are locally conformable. A larger, map-scale exposure of the formation occurs in the

Table 1. Summary of Thermobarometry Results From Loma de Las Chacras

Sample	Location	Coordinates Latitude, Longitude	Pressure kbar	±2σ	Temperature °C	±2σ	sfit	Phases
			Rio Las Chacras Formation					
Schist								
LLC39-3	Figure 4	31°13′51″S, 67°33′03″W	12.4	1.5	722	36	0.69 (1.73)	Grt-Bt-Ms-Plg-Qtz-H_2O
LLC39-5	Figure 4	31°13′46″S, 67°32′51″W	12.1	1.4	713	33	0.51 (1.73)	Grt-Bt-Ms-Plg-Qtz-H_2O
LLC40-4	Figure 3	31°17′10″S, 67°31′48″W	12.4	1.5	735	41	0.50 (1.73)	Grt-Bt-Ms-Plg-Qtz-H_2O
Amphibolite								
LLC30-7	Figure 3	31°13′24″S, 67°32′48″W	12.4	1.6	643	46	1.38 (1.73)	Grt-Amp-Plg-Ep-Qtz-H_2O
LLC39-4	Figure 4	31°13′42″S, 67°32′50″W	11.8	2.0	759	66	0.74 (1.73)	Grt-Amp-Plg-Ep-Qtz-H_2O
LLC40-4	Figure 3	31°17′10″S, 67°31′48″W	13.4	1.5	731	97	0.10 (1.96)	Grt-Amp-Plg-Qtz-H_2O
			Villarcan Gneiss					
LLC28-8 (Matrix)	Figure 4	31°13′26″S, 67°32′12″W	10.7	2.2	900	80	1.38 (1.63)	Grt-Bt-Mu-Plg-Ky-Qtz-H_2O
LLC28-8 (Inclusions)	Figure 4	31°13′26″S, 67°32′12″W	9.1	1.9	734	109	1.73 (1.73)	Grt-Bt-Plg-Ky-Qtz-H_2O
LLC39-6 (Matrix)	Figure 4	31°14′13″S, 67°33′20″W	11.4	1.9	894	48	0.91 (1.73)	Grt-Bt-Plg-Ky-Qtz-H_2O
LLC39-6 (Inclusions)	Figure 4	31°14′13″S, 67°33′20″W	6.5	2.2	632	50	0.91 (1.73)	Grt-Bt-Plg-Ky-Qtz-H_2O
LLC39-7	Figure 4	31°14′19″S, 67°33′42″W	12.5	2.4	815	57	1.73 (1.73)	Grt-Bt-Plg-Ky-Qtz-H_2O

eastern end of Quebrada Villarcan (Figure 4) where the unit is interpreted to intrude the Villarcan Gneiss.

2.2. Ductile Shear Zones

[12] *Vujovich* [1994] recognized the presence of mylonite and ultramylonite within the Las Chacras region, but no workers have attempted a detailed study of individual shear zones and their relation to metamorphic history of the region. We recognize several first-order structures that bound the major units described above.

[13] The Don Juan shear zone in the southeast (Figure 3) and Flechal shear zone in the northeast (Figure 4) separate the Don Juan Formation in the hanging wall from the Villarcan Gneiss and Rio Las Chacras Formation in the footwall (Figure 4). Well-developed mylonite and ultramylonite (Figure 5h) dip moderately to the southeast (Don Juan shear zone) and to the northeast (Flechal shear zone). Within the footwall of both shear zones, coarse (< 0.5 cm) mica overgrows previous foliation and lineation within the Villarcan Gneiss. The shear zones are truncated along strike to the east by an active brittle fault zone of the Valle Fertil lineament. The hanging wall foliation is folded by a set of northeast plunging folds. Kinematic indicators (asymmetric tails on porphyroclasts, mica fish, and quartz fabrics) show top-to-the-southeast sense of motion within the Don Juan shear zone and top-to-the-northeast sense of motion within the Flechal shear zone (Figure 5h).

[14] The Rio Las Chacras shear zone in the southeast (Figure 3) and the Villarcan shear zone in the northwest (Figure 4) separate Villarcan Gneiss in the footwall from the Rio Las Chacras Formation in the hanging wall. At the lowest structural levels pelitic protoliths within the Villarcan Gneiss preserve a stromatitic texture (Figure 5d) with a moderate foliation (S_A) defined by alternating bands of leucosome and melanosome as well as aligned biotite and kyanite within the melanosome itself. The mineral lineation (L_A), defined by aligned mica and kyanite, plunges shallowly toward 340° and 150° (Figure 2). Approximately 600–700 m structurally beneath the Villarcan shear zone, the foliation and lineation intensify such that stromatitic layering is overprinted by an intense gneissic layering subparallel to the shear zone (Figure 5e).

[15] Two sets of isoclinal folds deform the Rio Las Chacras and Villarcan shear zones (Figure 4). The first (F_A) plunges shallowly to the northwest-southeast and fold axes trend subparallel to L_A (Figure 2). The second fold set (F_B) plunges shallowly to northeast-southwest and folds both F_A and Villarcan shear zone. Similar fabrics exist within the Rio Las Chacras shear zone but are difficult to distinguish due to overprinting fabrics associated with the structurally overlying Don Juan shear zone.

2.3. Summary

[16] The outcrop geology suggests that intrusion of the mafic-ultramafic La Vibora formation and migmatization within the Villarcan Gneiss predates deformation on the Villarcan and Rio Las Chacras shear zones. The La Vibora formation intrudes the migmatites of the Villarcan Gneiss, and the latter are overprinted by fabrics associated with the Villarcan and Rio Las Chacras shear zones. The shear zones were synchronous with or post date metamorphism within the Rio Las Chacras Formation and were followed by two generations of isoclinal recumbent folding (F_A and F_B). The last stages of ductile deformation involved top-down sense of motion on the Don Juan and Flechal shear zones followed by regional open and upright folding (F_C).

3. Petrology and Thermobarometry

[17] We selected samples throughout Las Chacras in order to (1) compare the metamorphic conditions of the various units and to assess if any breaks in pressure and/or temperature occur across major structures, (2) determine the pressure-temperature path of the Villarcan Gneiss with respect to that of granulite facies migmatites of the Famatina margin east of the Valle Fertil lineament, and (3) determine of the conditions of metamorphism and migmatization within the Rio Las Chacras Formation. The Don Juan Formation lacks suitable assemblages for thermobarometry and is therefore not discussed below. Mineral compositions were determined by electron probe microanalysis using a Cameca SX-100 at UC, Davis and a Cameca SX-51 at UC Berkeley. Natural and synthetic materials were used as standards.

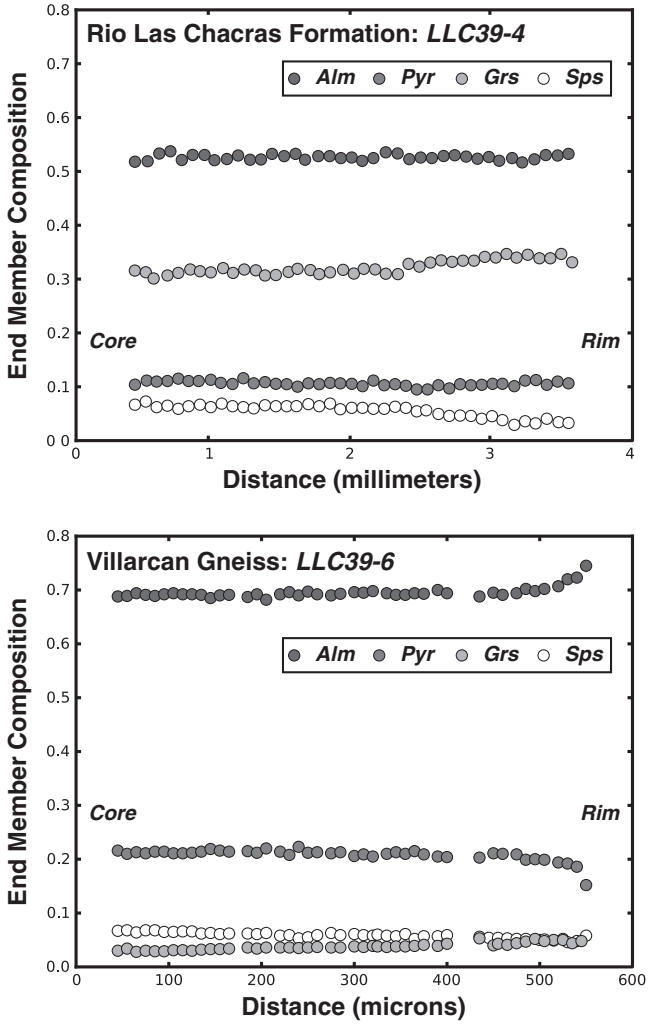

Figure 7. Core to rim garnet zoning profiles from (a) the Rio las Chacras amphibolite and (b) stromatitic migmatite of the Villarcan Gneiss.

An accelerating voltage of 15 kV was used for all analyses; a 1 μm beam was used for garnet, amphibole, and epidote; and 10 μm beam was used for analyses of plagioclase, muscovite, and biotite. Mineral compositions are provided in Appendix A. Pressure and temperature conditions were estimated by the average PT method [*Powell and Holland*, 1994] using the most recent version of the software THERMOCALC. Mineral activities were calculated with the accompanying software AX.

3.1. Rio Las Chacras Formation

[18] Schist within the Rio Las Chacras Formation contains the assemblage Ms-Bt-Grt-Plg-Qtz ± Ky. Garnet is Fe rich (XAlm ~ 0.68), generally lacks compositional zoning, and is often poikilitic with inclusions of mica, quartz, and plagioclase. THERMOCALC average PT calculations were performed using the assemblage Grt-Bt-Ms-Pl with Qtz and H_2O in excess. Three samples were selected from the Rio Las Chacras formation within the hanging walls of the Villarcan and Rio Las Chacras shear zones (Table 1 and Figures 3 and 4). Using garnet rims and matrix mineral compositions, all three samples are consistent with weighted average PT conditions of 12.3 ± 0.9 kbar and 722 ± 21°C that we interpret as peak metamorphic conditions.

[19] Amphibolite from within the Rio Las Chacras Formation contains the assemblage Amp-Grt-Czo-Pl-Qtz-Ttn ± Rt. Three samples of the Rio Las Chacras amphibolite were selected for thermobarometry. Average PT conditions were calculated using the assemblage Grt-Amp-Czo-Plg with Qtz and H_2O in excess. Garnet is Fe rich (XAlm ~0.53) and displays weak prograde zoning, particularly in Mn, which is elevated in the core and decreases toward the rim (Figure 7). Amphibole compositions are more restricted than within the Don Juan Formation and Villarcan Gneiss and range from magnesiohornblende to tschermakite (Figure 8a). The restricted range of Ti and Al compositions of the amphiboles (Figure 8b) qualitatively suggests metamorphic temperatures intermediate between the Don Juan Formation and Villarcan Gneiss [e.g., *Ernst and Liou*, 1998]. Using garnet rims and matrix mineral compositions, all three samples result in PT estimates that are consistent with weighted average PT conditions of 12.7 ± 0.9 kbar and 688 ± 35°C that we interpret as peak metamorphic conditions.

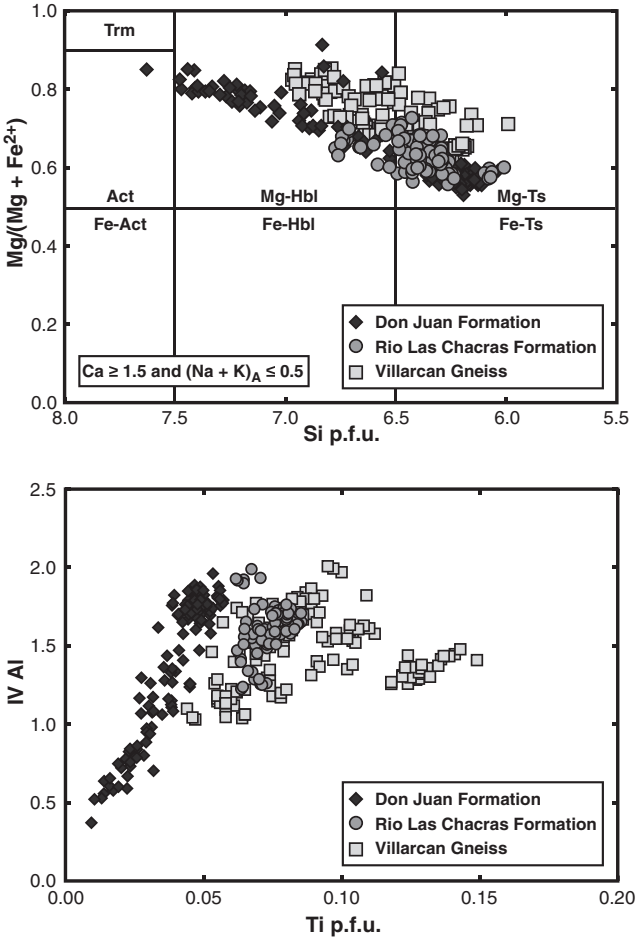

Figure 8. Amphibole composition diagrams for amphibolites from the Don Juan Formation, Rio Las Chacras Formation, and Villarcan Gneiss. Trm = termolite, Act = actinolite, Fe-Act = ferroactinolite, Mg-Hbl = magnesiohornblene, Fe-Hbl = ferrohornblende, Mg-Ts = magnesiotschermakite, Fe-Ts = ferrotschermakite. See text for discussion.

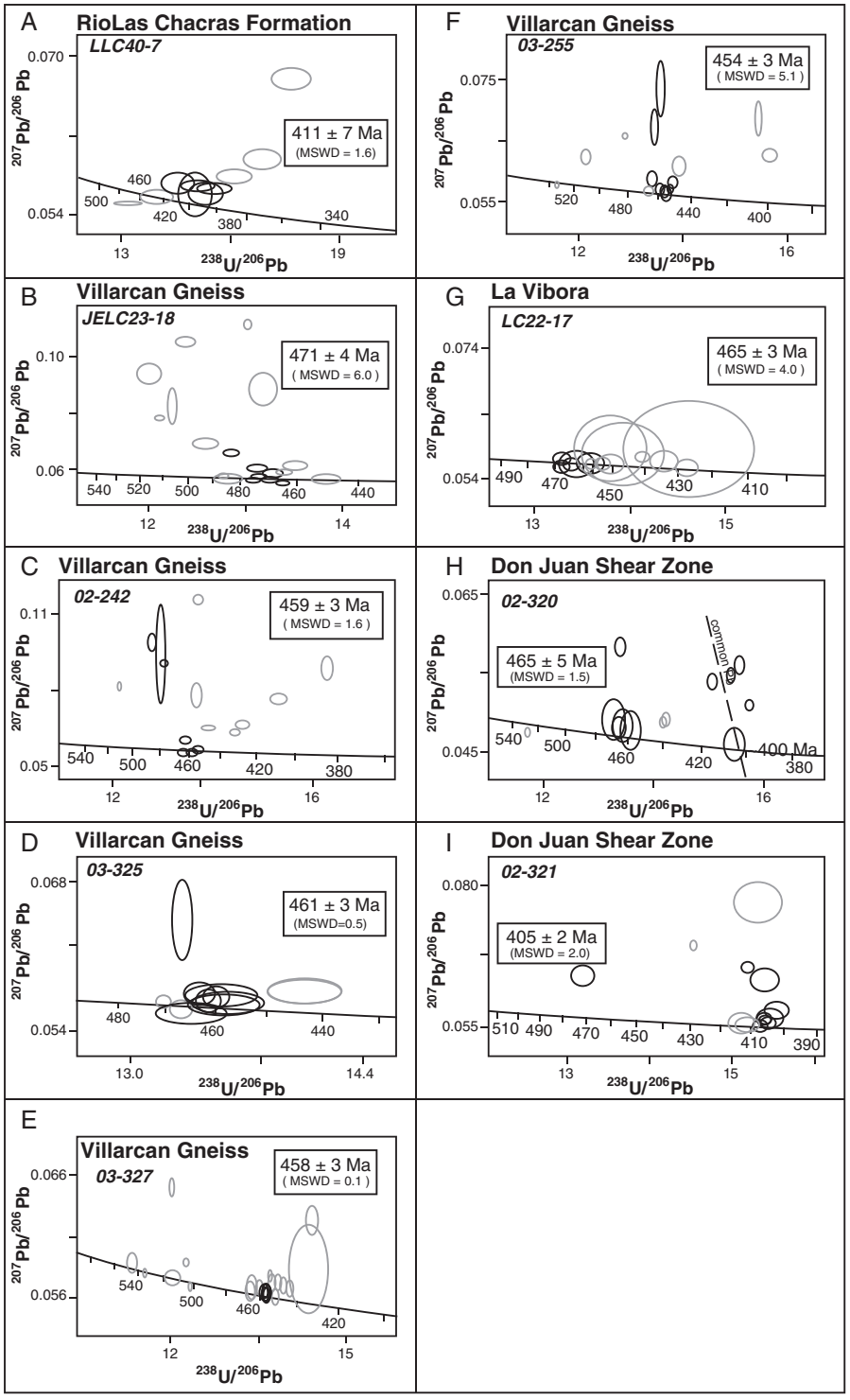

Figure 9. U-Pb zircon concordia diagrams for zircon samples: (a) trondhjemite sill that intrudes Rio Las Chacras amphibolite, sample LLC40-7, (b) L-tectonite orthogneiss within the Villarcan Gneiss, sample JELC23-18, (c) strongly foliated granitoid within the Villarcan Gneiss, sample 02-242, (d) stromatitic leucosome of kyanite–K-feldspar migmatite of the Villarcan Gneiss, sample 03-225, (e) amphibolite body within the Villarcan Gneiss, sample 03-327, (f) tonalite that intrudes the Villarcan Gneiss, sample 03-255, and (g) La Vibora metagabbro, sample LC22-17.

Table 2. Summary of Geochronology Results From Loma de Las Chacras

Sample	Unit	Location	Coordinates (Latitude, Longitude)	Age (Ma)	±	MSWD	Comments
			U-Pb Zircon				
LLC40-7	Rio Las Chacras Formation	Figure 4	31°13′29″S, 67°32′38″W	411	7	1.6	Crystallization age
JELC23-18	Villarcan Gneiss	Figure 4	31°13′21″S, 67°31′26″W	471	4	6.0	Inferred crystallization age
02-242	Villarcan Gneiss	Figure 3	31°17′47″S, 67°32′32″W	459	3	1.6	Crystallization age
03-325	Villarcan Gneiss	Figure 4	31°14′37″S, 67°34′15″W	461	3	0.5	Crystallization age
03-327	Villarcan Gneiss	Figure 4	31°14′35″S, 67°34′11″W	458	3	0.1	Crystallization age
03-255	Villarcan Gneiss	Figure 1	31°15′29″S, 67°31′01″W	454	3	5.1	Inferred crystallization age
02-320	Villarcan Gneiss	Figure 3	31°16′07″S, 67°30′48″W	461	5	1.5	Crytsallization age
02-321	Villarcan Gneiss	Figure 3	31°15′53″S, 67°31′00″W	405	2	2.0	Crystallization age
LC22-17	La Vibora	Figure 4	31°32′17″S, 67°13′41″W	465	3	4.0	Inferred crystallization age
			U-Pb Titanite				
LLC38-11	Villarcan Gneiss	Figure 1	31°16′45″S, 67°33′16″W	407	11	17.0	Inferred metamorphic age
			Lu-Hf Garnet				
LLC39-4	Rio Las Chacras Formation	Figure 4	31°13′42″S, 67°32′50″W	407	1.3	1.6	Metamorphic age
LLC39-6	Villarcan Gneiss	Figure 4	31°14′13″S, 67°33′20″W	434	17	0.34	Cooling age
			$^{40}Ar/^{39}Ar$ *Amphibole*				
LC6-19	Don Juan Formation	Figure 3	31°17′49″S, 67°30′47″W	≥ 422			Maximum age
				≥ 425			Maximum age
LLC39-4	Rio Las Chacras Formation	Figure 4	31°13′42″S, 67°32′50″W	≥427			Maximum age
				≥ 433			Maximum age.
				407	11	1.4	Inverse isochron age (p = 0.10).
LLC16-1	Rio Las Chacras Formation	Figure 3	31°16′11″S, 67°31′01″W	439	10	2	Inverse isochron age (p = 0.06)
LLC10-2	Villarcan Gneiss	Figure 4	31°14′35″S, 67°34′11″W	673	9		Integrated age
				681	9		Integrated age
			$^{40}Ar/^{39}Ar$ *Biotite*				
LLC10-2	Villarcan Gneiss	Figure 4	31°14′35″S, 67°34′11″W	432	8	1.40	Plateau age (p = 0.20)
				432	8	0.58	Plateau age (p = 0.81)
				445	7	1.14	Mini-plateau age (p = 0.34)
				444	6	2.13	Mini-plateau age (p = 0.05)
				373	26	1.0	Inverse isochron age (p = 0.44)

3.2. Villarcan Gneiss

[20] Three samples of migmatite melanosome from the Villarcan Gneiss were selected for thermobarometry. Randomly aligned muscovite locally occurs at the contact between the melanosome and leucosome. Garnet contains inclusions of kyanite, biotite, plagioclase, and quartz (Figure 6c). Kyanite and biotite define a microscale foliation that is deformed by the earliest episode of folding (Figure 6d). Garnet displays relatively uniform composition except for minor deflections within 50–75 μm of the rim, which display increased Grs and Alm and decreased Pyr (Figure 7). The Sps component generally decreases from core to rim. Garnet compositions from analyses with the highest X_{Mg} were combined with matrix biotite and plagioclase. Average PT conditions were calculated with the assemblage Grt-Bt-Ms-Plg-Ky-Qtz. The three samples produced similar results (Table 1) consistent with migmatization at 11.5 ± 1.2 kbar and 868 ± 33°C.

[21] Two samples contained biotite, plagioclase, kyanite, and quartz as inclusions within garnet. Estimates of pressure and temperature were calculated by combining the garnet core composition with the compositions of included biotite and plagioclase, which resulted in conditions of 9.1 ± 1.9 kbar and 734 ± 101°C for sample LLC28-8 and 6.5 ± 2.2 kbar and 632 ± 50°C for sample LLC39-6 (Table 1). The possibility that inclusion compositions were reset after granulite facies metamorphism cannot be excluded; however, the temperature estimates are consistent with pregranulite facies temperatures east of the Valle Fertil lineament.

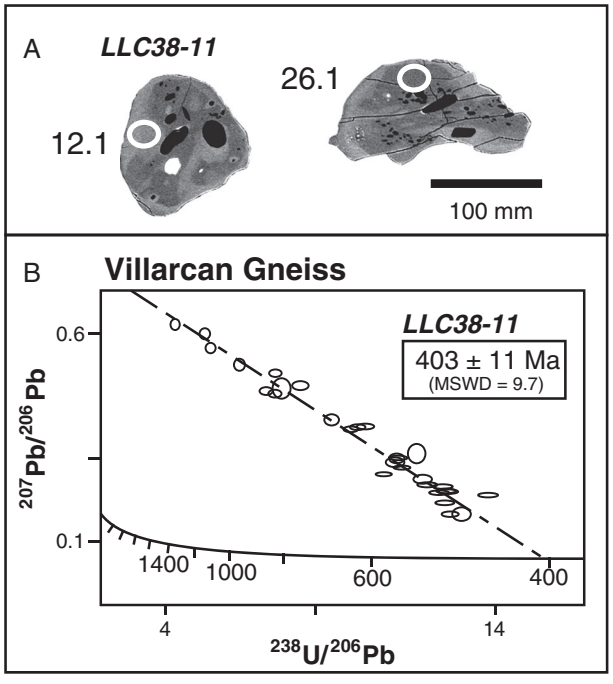

Figure 10. Backscattered electron image and U-Pb concordia diagram from titanite within amphibolite of the Villarcan Gneiss, sample LLC38-11.

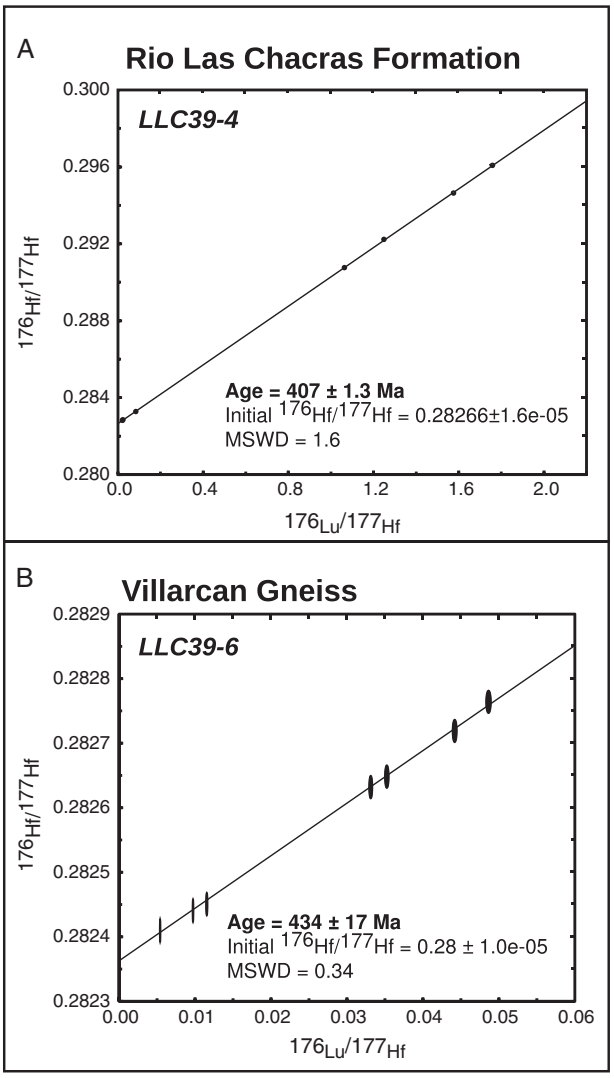

Figure 11. Lu-Hf isochron for samples LLC39-4 and LLC39-6, from the Rio Las Chacras amphibolite and Villarcan Gneiss migmatite, respectively.

[22] Amphibolites within the Villarcan Gneiss generally contain the assemblage Amp-Czo-Plg-Qtz-Ttn ± Bt. Amphiboles range in composition from magnesiohornblende to tschermakite. The amphiboles exhibit a range in composition with $0.05 \geq$ Ti (p.f.u.) ≥ 0.15 and qualitatively suggest that at least some samples preserve a higher temperature history than those from the Rio Las Chacras and Don Juan Formations (Figure 8). The amphibolites generally lack suitable assemblages for estimating the pressure of metamorphism. We selected four samples for hornblende-plagioclase thermometry following the method of *Holland and Blundy* [1994]. Two samples, LC23-9 and LLC10-2, come from amphibolites interlayered with stromatitic Grt-By-Ky ± Kfs ± Qtz migmatite in the south and north, respectively (Figures 3 and 4). Both samples record temperatures of 770 ± 50°C within the kyanite stability field, consistent with the temperature estimates of pelitic migmatites above. Two samples, LC23-10, LC24-10 (Figures 1 and 3), were sampled from amphibolite within the Villarcan Gneiss that is overprinted by lower grade fabrics associated with the Don Juan shear zone. The samples give equivalent temperatures of 630 ± 50°C within the kyanite stability field.

3.3. Summary

[23] The data indicate that the Rio Las Chacras Formation and Villarcan Gneiss record distinctly different metamorphic histories. Within the Rio Las Chacras formation, garnet in amphibolite preserves prograde zoning, amphibole has relatively limited compositional range, and peak metamorphic temperatures are ~650–700°C. The formation records only a single metamorphic event. The PT conditions, metamorphic assemblage, and low melt volume are consistent with melting of muscovite under vapor-saturated conditions via the reaction Ms + Qtz + H_2O = Ky + liquid [e.g., *Spear et al.*, 1999]. In contrast, garnet within the Villarcan Gneiss displays zoning consistent with diffusional resetting, peak metamorphic temperatures are ~800°C, and amphibolites record metamorphic conditions from peak temperatures down to lower temperatures of ~630°C. Inclusion assemblages preserved in garnet indicate lower pressures and temperatures preceded granulite facies metamorphism. The PT conditions, the general lack of muscovite and low abundance of K-feldspar within the migmatite melanosome, and large (≥ 25–30%) melt volume observed in outcrop are consistent with a muscovite dehydration melting reaction Ms + Qtz = Ky + Kfs + liquid [e.g., *Spear et al.*, 1999]. The data from the Villarcan Gneiss record a counterclockwise pressure temperature path that involved (1) increasing pressure and temperature from ~7 to 9 kbar and ~630–750°C culminating in (2) peak granulite facies metamorphism and migmatization at ~11.5 kbar and ~868°C, and followed by (3) cooling to temperatures of ~630°C.

4. Geochronology

[24] The structural history and metamorphic conditions indicate that the individual units within Las Chacras experienced distinctly different metamorphic histories. In order to determine the timing and duration of magmatism, metamorphism, and deformation within Las Chacras with respect to the regional events, we have conducted U-Pb zircon and titanite geochronology, Lu-Hf garnet geochronology, and $^{40}Ar/^{39}Ar$ thermochronology from selected samples from the major units in the Las Chacras area. The ages are summarized in Table 2.

4.1. U-Pb Geochronology

[25] A wide array of intrusive bodies and migmatitic leucosomes provide an opportunity to define the timing of magmatism and metamorphism in Las Chacras. Samples were collected from igneous and metamorphic intrusions from the major units for U-Pb zircon analysis. In addition, we separated titanite from amphibolites within the Rio Las Chacras formation and Villarcan Gneiss for U-Pb analysis to estimate the timing of metamorphism and age of cooling from high temperature. All samples were analyzed using the SHRIMP-RG at the USGS-Stanford University ion probe laboratory. Analytical methods, CL images, and U-Pb isotopic data are provided Appendix B.

4.1.1. Zircon

[26] Sample LLC40-7 was collected from a trondjhemitic sill within the Rio Las Chacras amphibolite (Figure 4). The

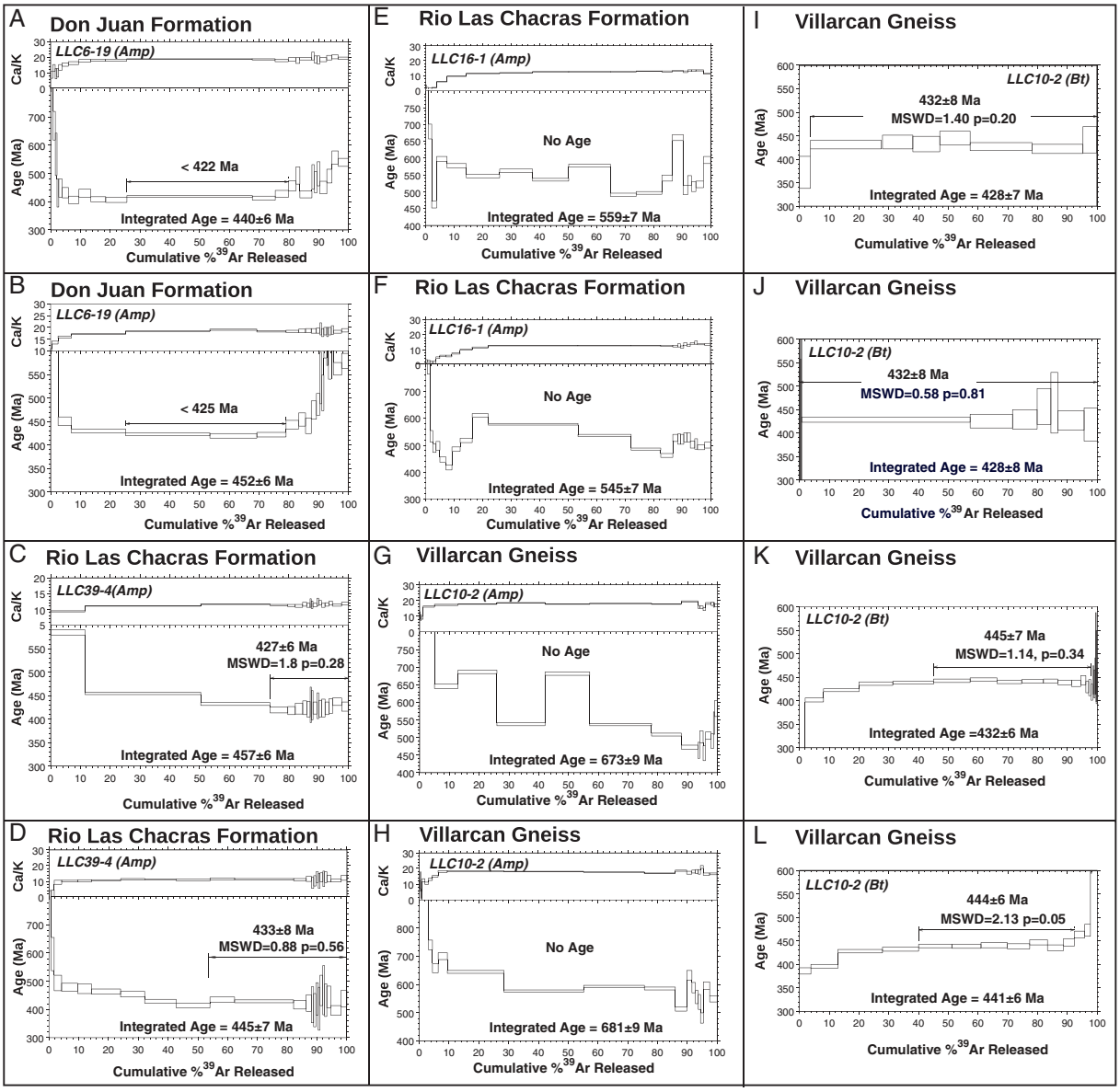

Figure 12. $^{40}Ar/^{39}Ar$ age spectra for Loma de Las Chacras samples: (a and b) amphibole spectra from rare amphibolite from the Don Juan Formation, (c and d) amphibole sprectra from Grt-Czo amphibolite from the Rio Las Chacras Formation in the northern portion of the region, (e and f) amphibole sprectra from Grt-Czo amphibolite from the Rio Las Chacras Formation in the southern portion of the region, (g and h) amphibole spectra, and (i–l) biotite spectra from Bt amphibolite of the Villarcan Gneiss.

sill is deformed by second generation folds (F_B) that exhibit irregularly thinned limbs and thickened hinges (Figure 5b) suggesting that magmatism was synchronous with folding. Zircon from the sill is subequant to elongate with cores surrounded by oscillatory zoned, 10 to 40 μm thick rims. Two Mesoproterozoic grains record obvious xenocrysts. The five youngest analyses have high common Pb values and are interpreted to have suffered from Pb loss. Excluding two analyses with high U, the five remaining concordant to nearly concordant analyses give a weighted mean $^{206}Pb/^{238}U$ age of 411 ± 7 (MSWD = 1.6) that is interpreted as the age of crystallization (Figure 9a).

[27] An intermediate orthogneiss collected from the eastern margin of the range (JELC23-18; Figure 4) yielded a population of small euhedral zircon characterized by cores overgrown by oscillatory zoned mantles and CL-dark, high-U rims or well developed tips. Two core analyses (1.1, 4.1) are clearly older and indicate the presence of inherited components. The remaining $^{206}Pb/^{238}U$ ages from the cores, mantles, and rims range from 600 to 445 Ma. Many of the older and younger ages have high common Pb values. Seven analyses from the mantle domain with low common Pb give a weighted mean age of 471 ± 4 Ma (MSWD = 6) (Figure 9b). We tentatively interpret this as the magmatic age for this sample. Older ages from both mantle and rim domains are inferred to reflect mixtures with the core domain, while the younger age distribution is attributed to continued metamorphism.

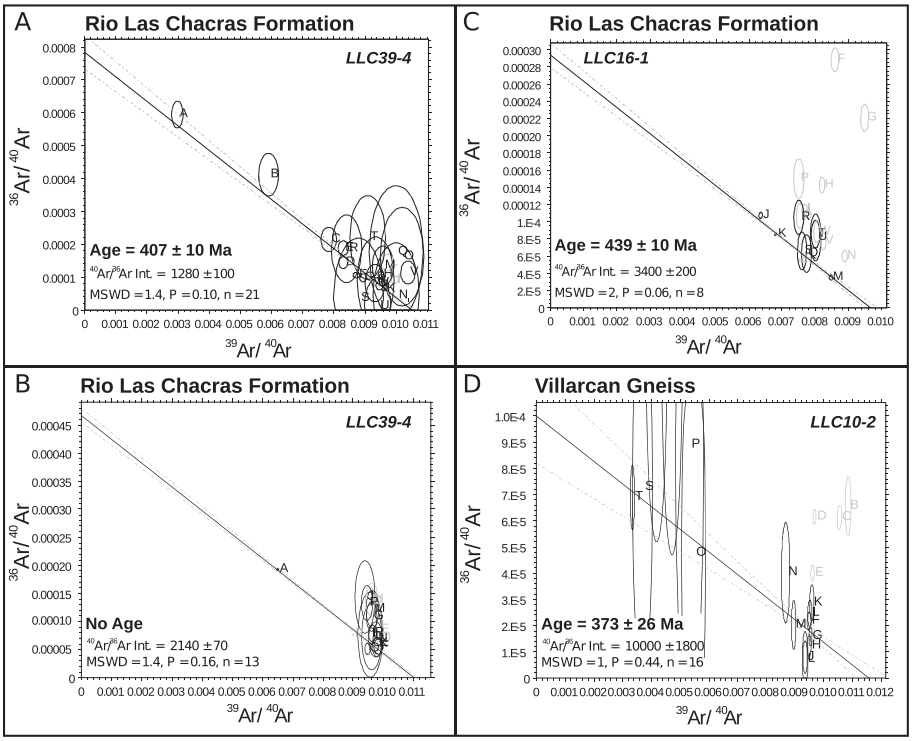

Figure 13. $^{40}Ar/^{39}Ar$ inverse isochrons for Loma de Las Chacras samples: (a and b) amphibole from Grt-Czo amphibolite from the Rio Las Chacras Formation in the northern portion of the region, (c) amphibole from Grt-Czo amphibolite from the Rio Las Chacras Formation in the southern portion of the region, and (d) biotite from Bt amphibolite of the Villarcan Gneiss.

[28] Sample 02-242 was collected from a leucogranite dike within the Villarcan Gneiss in the southwest portion of Las Chacras (Figure 3). Zircons from the dike are elongate and euhedral with CL-dark, high-U metamict cores overgrown by oscillatory zoned rims. The cores contain patchy recrystallized domains that have the same CL response as the rims. One analysis of the dark core domain gave an age of 396 Ma. Another 17 analyses of the rim domain gave ages from 464 to 368 Ma. The seven oldest rim analyses define a $^{206}Pb/^{238}U$ weighted mean age of 459 ± 3 Ma (MSWD = 1.6) (Figure 9c) that we interpret as the age of crystallization for the leucogranite. The high-U cores are interpreted to be extensively recrystallized xenocrystic zircon. Younger rim ages are inferred to record Pb loss due to continued metamorphism and deformation.

[29] Granulite facies metapelites of the Villarcan Gneiss are migmatitic with abundant leucosomes. A sample of leucosome (03-325; Figure 4) produced a complex population of small zircon ranging from euhedral oscillatory zoned grains to subequant grains with round cores overgrown by high-U rims. The round cores generally give Mesoproterozoic $^{207}Pb/^{206}Pb$ ages and are interpreted as detrital components derived from the metapelite. The euhedral grains and rims yield younger ages ranging from 470 to 330 Ma with most centering round 460 Ma. Eight concordant analyses give a $^{206}Pb/^{238}U$ weighted mean age of 461 ± 3 Ma (MSWD = 0.5; Figure 9d). We interpret this as the age of leucosome crystallization and attribute the younger ages to Pb loss or continued metamorphism or fluid activity.

[30] A trondhjemitic sill within boudinaged amphibolite of the Villarcan Gneiss was collected from the western margin of Quebrada Villarcan (Sample 03-327; Figure 4). Elongate zircon from the sample consisted of high-U ($\geq$ 2000 ppm) metamict cores overgrown by oscillatory mantles and 5–15 μm thick outer low-U rims. The metamict cores generally give older $^{206}Pb/^{238}U$ ages ranging from 500 to 740 Ma and become reversely discordant when corrected for common Pb. The mantle over-growths have low Th (29–116 ppm) and low Th/U ($\leq$ 0.1) with $^{206}Pb/^{238}U$ ages of 443–465 Ma. Six concordant analyses define a concordia age of 458 ± 3 Ma (MSWD = 0.1) that we interpret as the magmatic age (Figure 9e). The older ages are interpreted as mixed domains involving the metamict cores, and the younger ages are interpreted to reflect younger metamorphism recorded by the outer rims at ~430 Ma.

[31] A sample of a 5 cm thick tonalite dike that intrudes an amphibolite in the Villarcan Gneiss (sample 03-255; Figure 1) contained a complex zircon population dominated by round oscillatory zoned cores overgrown by oscillatory zoned high-U rims. Core analyses vary from concordant with ages ranging from 515 to 1225 Ma to strongly discordant. The rims give ages ranging from 395 to 485 Ma, assuming that older rim ages reflect mixtures of core and rim domains. Eight rim analyses define a $^{206}Pb/^{238}U$ weighted mean age of 454 ± 3 Ma (MSWD = 5.1). Alternatively, the older ages can be interpreted to reflect an emplacement age of 470–480 Ma and the spread of younger ages attributed to continued metamorphism down to ~400 Ma (Figure 9f).

[32] Sample 02-320 was collected from a granitic orthogneiss that is overprinted by deformation fabrics of the Don Juan shear zone. A complicated suite of zircons from this sample includes grains with obvious xenocrystic

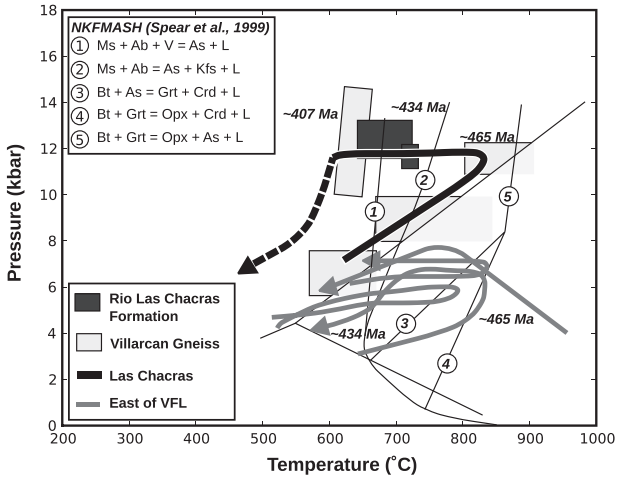

Figure 14. Pressure-temperature-time path for the Villarcan Gneiss and Rio las Chacras Formations. Mineral reaction curves are taken from [*Spear et al.*, 1999].

cores overgrown by oscillatory zoned mantles and euhedral oscillatory zoned grains. Most grains have a 2–20 μm thick CL-dark, high-U rims that are thickest at the grain tips. The cores give concordant ages ranging from 1.0 to 1.2 Ga and some discordant analyses interpreted as mixed ages from older cores and younger mantles. Many of the oscillatory zoned zircon give discordant analyses interpreted to reflect the combined effects of Pb loss and or mixed analysis of older and younger domains. Five concordant to nearly concordant analyses define a $^{206}Pb/^{238}U$ weighted mean age of 461 $\pm$ 5 Ma (MSWD = 1.5). Five distinct rim and tip analyses give $^{206}Pb/^{238}U$ ages ranging from 410 to 395 Ma, whereas others give older ages assumed to be from mixed domains or younger ages that reflect Pb loss. The older age of $\sim$461 Ma is interpreted as the crystallization age for the granite, and the younger rims are related to metamorphism and deformation at $\sim$ 400 Ma.

[33] Sample 02-321 was collected from a trondhjemite pegmatite in the neck of an amphibolite boudin within the Don Juan shear zone. The zircon is euhedral, oscillatory zoned, and displays thin rims with lower U. Approximately 10% of the grains have xenocrystic cores that yield older ages. Thirteen analyses of oscillatory zoned zircon give an age of 405 $\pm$ 2 Ma (MSWD = 2) that we interpret as the age of crystallization for the trondhjemite.

[34] Sample LC22-17 was collected from the La Vibora metagabbro that intruded the Villarcan Gneiss in the eastern portion of Quebrada Villarcan (Figure 4). Zircons from the sample are subequant to elongate with oscillatory zoned cores overgrown by 10 to 20 μm thick, CL-bright rims. Six of twelve core analyses give a concordia age of 465 $\pm$ 3 Ma (MSWD = 4.0). The remaining analyses spread continuously down to the youngest low-U rim age of $\sim$425 Ma (Figure 9g). We interpret the concordia age as the crystallization age for the gabbro and the younger ages to reflect continued metamorphism and/or deformation.

[35] The zircon U-Pb ages reveal distinctly different magmatic histories for the Rio Las Chacras Formation and the Villarcan Gneiss. Melting occurred within the Rio Las Chacras Formation at $\sim$411 Ma. In contrast magmatic ages from the Villarcan Gneiss span from $\sim$454 to $\sim$472 Ma. The timing of mafic and intermediate intrusions was synchronous with crystallization of migmatitic leucosome in the Villarcan Gneiss. This observation combined with a counterclockwise pressure-temperature path is consistent with a model of migmatization driven by the melt intrusion. The timing and magnitude of peak metamorphic conditions are consistent with Las Chacras representing the lower crustal equivalent of middle crustal granulite facies migmatites to the east of the Valle Fertil lineament. Younger rims on zircon suggest that the Villarcan Gneiss may have been affected by later metamorphic or deformation events at $\sim$425 and $\sim$400 Ma, approximately coeval with the melting in the Rio Las Chacras Formation. Zircon rim and core ages of $\sim$405 Ma date top-to-east extension within the Don Juan shear zone.

4.1.2. Titanite

[36] Titanite was separated from four samples: two samples of Grt-Czo amphibolite of the Rio Las Chacras Formation from the hanging wall of the Rio Las Chacras shear zone (Sample LLC16-1; Figure 3) and Villarcan shear zone (Sample LLC39-4; Figure 4) and two samples of amphibolite in the Villarcan Gneiss. Sample LLC28-8 was collected adjacent to the La Vibora intrusion in the eastern portion of Quebrada Villarcan (Figure 4). Sample LLC38-11 was collected from a stromatitc migmatite from the southwest portion of the range (Figures 2 and 6f). Titanite in both Villarcan Gneiss samples is intergrown with and replaces ilmenite that replaces rutile. Individual grains are characterized by mottled cores and well-developed rims and contain abundant inclusions (Figure 10a). Titanite from the Rio Las Chacras Formation is compositionally homogeneous and has few inclusions.

[37] Titanite analyses from sample LLC38-11 have U concentrations of 8–175 ppm and $^{206}Pb/^{204}Pb$ ratios 30-255. Low U and high common Pb abundances preclude meaningful age determination for the three other samples. Common Pb correction for sample LLC38-11 was made using the measured $^{206}Pb/^{204}Pb$ ratios and the three-dimensional total Pb method of *Ludwig* [1998]. The linear solution [*Ludwig*, 2003] used a simple mixture of common and radiogenic Pb in titanite. There is no discernible age difference between the lower U cores and higher U rims. Regression of all 29 titanite analyses gives a lower intercept age of age of 407 $\pm$ 11 Ma (Figure 10b).

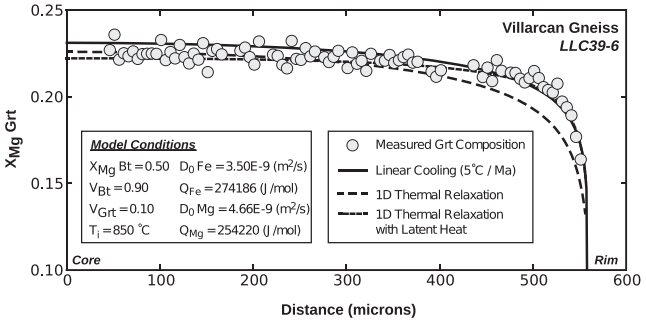

Figure 15. Modeled diffusion profiles for X_{Mg} in garnet from migmatites of the Villarcan Gneiss using a linear cooling rate of 5°C/ Ma and the cooling histories derived from one-dimensional step-shaped temperature distribution as in Figure 16.

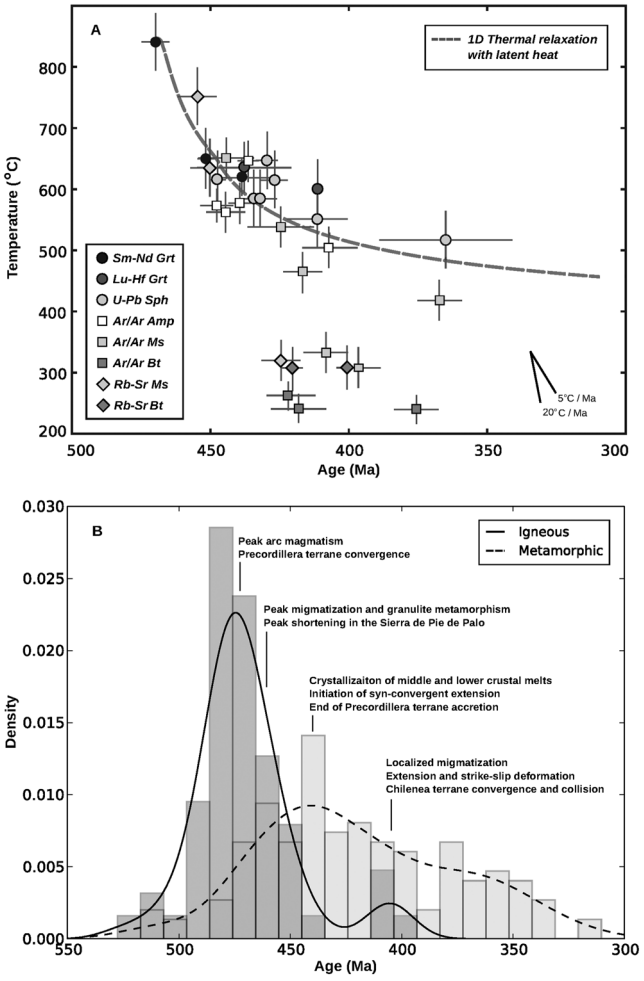

Figure 16. (a) Modeled cooling history for regional granulites of the Famatina arc derived from one-dimensional step-shaped temperature distribution [e.g., *Stüwe*, 1995]. (b) Distribution of regional magmatic and metamorphic/cooling ages from the Famatina margin. Isotopic ages are taken from literature and the sources are reported in the supporting information.

[38] The titanite age is significantly younger than the age of peak metamorphism in the Villarcan Gneiss. Replacement of rutile by ilmenite and titanite in the sample is consistent with a PT path of decreasing pressure and temperature. The age is interpreted to record cooling of the Villarcan Gneiss to below the accepted closure temperature for Pb in titanite of ~650°C [e.g., *Cherniak*, 1993] by ~407 Ma, approximately coeval with extension along the Don Juan shear zone.

4.2. Lu-Hf Geochronology

[39] We present Lu-Hf isotope data from an amphibolite of the Rio Las Chacras formation and from migmatite melanosome within the Villarcan Gneiss in order to date the timing of metamorphism and constrain the cooling history within both units. Four garnet and three garnet-free whole rock separates were analyzed from each sample. Sample Lu-Hf chemistry and analysis of isotopic compositions using the Thermo-Finnigan NEPTUNE were performed at Washington State University. Dissolution procedures and Lu-Hf data for the garnet and whole rock separates are given in Appendix C, and an isochron for each sample is shown in Figure 7. Lu-Hf ages and ϵHf values were calculated using a value for the ^{176}Lu decay constant value of 1.867×10^{-11} a^{-1} [*Scherer et al.*, 2000; *Soderlund et al.*, 2004] and ^{176}Hf/^{177}Hf = 0.282785 and ^{176}Lu/^{177}Hf = 0.0336 for CHUR (chondrite uniform reservoir) [*Bouvier et al.*, 2008].

[40] Within the Rio Las Chacras Formation, amphibolite sample LLC39-4 was collected from the immediate hanging wall of the Villarcan shear zone (Figure 4). The sample contains a single population of garnet that records prograde metamorphism at 12.1 ± 1 kbar and 637 ± 37°C. The sample yielded an isochron age of 407.1 ± 1.3 (MSWD = 1.6) Ma with an initial ^{176}Hf/^{177}Hf ratio of 0.28266 (Figure 11a).

[41] Sample LLC39-6 was collected from the melanosome of stromatitic migmatite of the Villarcan Gneiss in the footwall of the Villarcan shear zone (Figure 4), which records PT conditions of 11.5 ± 0.8 kbar and 868 ± 47°C. The whole rock and garnet separates define an isochron age of 434 ± 17 Ma (MSWD = 0.34) and an initial ^{176}Hf/^{177}Hf ratio of 0.28000 (Figure 11b). The low ^{176}Lu/^{177}Hf ratios are likely due to abundant magnetite inclusions within the garnet, which contributed to the relatively low MSWD.

[42] The accepted closure temperature for Lu-Hf in garnet is generally taken to lie between ~540 and 700°C [e.g., *Scherer et al.*, 2000]; therefore, the age of ~407 Ma from the Rio Las Chacras formation records prograde garnet growth, while the age of ~434 Ma from migmatites of the Villarcan Gneiss reflects the cooling of garnet from granulite facies metamorphism.

4.3. ^{40}Ar/^{39}Ar Geochronology

[43] Samples were collected from amphibolites for ^{40}Ar/^{39}Ar geochronology to constrain the cooling history from peak metamorphic temperatures. Samples were analyzed at the Berkeley Geochronology Center. Methods are the same as *Mulcahy et al.* [2011] and described in Appendix D along with the isotopic data.

[44] Sample LC6-19 is from a rare amphibolite within the hanging wall of the Don Juan shear zone (Figure 3). Two separates are U-shaped, indicating excess argon, and fail to give a plateau age (Figures 12a and 12b). The bottom of the saddles yield apparent ages around ~422–425 Ma, taken as maximum ages.

[45] Sample LLC39-4 is from amphibolite of the Rio Las Chacras Formation in the immediate hanging wall of the Villarcan shear zone (Figure 4). Amphibole separates were taken from the same specimen used for U-Pb and Lu-Hf geochronology from above. Two separates show evidence of excess argon and converge toward apparent ages of ~427 Ma and ~433 Ma with 26% and 41% of the total ^{39}Ar released (Figures 12c and 12d). Both ages are taken as maximum ages. Both samples were plotted in the inverse isochron diagram (Figures 13a and 13b), with only one of them (Figure 13a) showing enough spread along the isochron to yield interpretable results. In the latter, excess ^{40}Ar* is further demonstrated by a ^{40}Ar/^{36}Ar intercept ratio of 1280 ± 100. The inverse isochron accounts for the excess argon in the age calculation and allows calculating an age of 407 ± 10 Ma.

[46] Sample LLC16-1 is from amphibolite of the Rio Las Chacras Formation in the immediate hanging wall of the

Rio Las Chacras shear zone (Figure 3). Amphibole separates were taken from the same specimen used for U-Pb geochronology from above. Age spectra from two separates show evidence for excess argon and failed to produce plateau ages (Figures 12e and 12f). An inverse isochron, however, resulted in an age of 439 ± 10 Ma (MSWD = 2, p = 0.06) with an initial $^{40}Ar/^{36}Ar$ = 3400 ± 200 (Figure 13c).

[47] Sample LLC10-2 is a boudinaged amphibolite body within the Villarcan Gneiss (Figure 5f) and is intruded by sample 03-327, a trondhjemitic sill with a U-Pb zircon age of 457 ± 1 Ma. Two amphibole separates from the sample failed to produce plateau or isochron ages probably due to heterogeneous excess ^{40}Ar* and converge toward an approximate maximum age of ∼500 Ma (Figures 12g and 12h). Four biotite separates were analyzed yielding two well-behaved plateau ages of 433 ± 8 Ma (MSWD = 1.40, p = 0.20), and 432 ± 8 Ma (MSWD = 0.58, p = 0.81) with 96% and 100% of the total ^{39}Ar released, respectively (Figures 12i and 12j). An inverse isochron for the latter of the two analyses resulted in an age of 373 ± 26 Ma (MSWD = 1.0, p = 0.40) with an initial $^{40}Ar/^{36}Ar$ = 10,000 ± 1800 (Figure 13d). The plateau ages and the inverse isochron age are taken as bracketing the maximum and minimum age for cooling through the closure temperature for biotite in this sample. Two additional grains (Figures 12k and 12l) yielded $^{40}Ar/^{39}Ar$ age spectra showing ^{40}Ar* loss, probably by thermally activated diffusion. The two spectra converged toward miniplateau ages of 445 ± 7 Ma (MSWD = 1.14, p = 0.34) and 444 ± 6 (MSWD = 2.13, p = 0.05).

[48] The data imply rapid cooling of the Rio Las Chacras Formation from peak metamorphic temperatures of ∼637°C to beneath the accepted closure temperature for the $^{40}Ar/^{39}Ar$ system in hornblende (∼550°C) at ∼407 Ma.

5. Discussion

5.1. Metamorphism and Deformation in the Loma de Las Chacras

[49] The above data require a more complex structural and metamorphic history for Las Chacras than previously recognized. The region contains migmatites from two distinct episodes of lower crustal melting preserved within discrete lithotectonic units that experienced different metamorphic, magmatic, and structural histories (Figure 14). Ordovician granulite facies metamorphism within the Villarcan Gneiss resulted from the intrusion of mafic and intermediate melts and culminated in peak metamorphic conditions of ∼850°C at lower crustal conditions of ∼12 kbar at ∼465 Ma. Our calculated PT conditions for the Villarcan Gneiss and age of migmatization are consistent with previous estimates [*Baldo et al.*, 2001; *Casquet et al.*, 2012]. Cooling from peak metamorphic conditions was nearly isobaric and resulted in a counterclockwise PT path. Slow cooling from peak metamorphic conditions is suggested by a garnet Lu-Hf ages of ∼434 Ma and a U-Pb titanite age of ∼407 Ma. In contrast, the Rio Las Chacras formation shows no evidence of experiencing Ordovician granulite facies metamorphism. Peak amphibolite facies metamorphism and melting within the formation occurred from ∼411–407 Ma as indicated by zircon U-Pb, garnet Lu-Hf, and amphibole $^{40}Ar/^{39}Ar$ ages. The data suggest that the two units were juxtaposed along the Rio Las Chacras–Villarcan shear zone by ∼407 Ma. The maximum age of metamorphism in the Don Juan Formation is constrained to be ∼421 Ma. Like the Rio Las Chacras Formation, the unit did not experience the Ordovician granulite facies event. The Rio Las Chacras–Villarcan shear zones are strongly overprinted by fabrics of the Don Juan–La Flechal shear zone, which experienced extension at ∼405 Ma as recorded by zircon ages of melt within extensional fabrics.

5.2. Regional Cooling From Ordovician Granulite Facies

[50] The metamorphic and magmatic history within the Villarcan Gneiss is consistent with granulite facies metamorphism to the east of Valle Fertil lineament. The counterclockwise PT path, age of migmatization, and age of mafic and intermediate intrusive bodies are equivalent. In contrast to granulite facies rocks to the east, which preserve midcrustal conditions of ∼5–7 kbar in the sillimanite stability field, the Villarcan Gneiss records metamorphism at lower crustal conditions of ∼12 kbar in the kyanite stability field (Figure 14). The combined data suggest that the middle and lower crust of the Famatina arc margin was isothermal (∼850°C) at ∼465 Ma. *Gallien et al.* [2010] estimated cooling rates between 3 and 6°C/Ma from ∼477 to 396 Ma; however, the number of data points and the regional extent of the data were limited. Despite the well-documented shape of the pressure-temperature paths and ages of peak metamorphism and migmatization, the duration that melt was present in the middle and lower crust and the cooling history from peak granulite conditions with respect to regional convergence and extension remains poorly constrained.

[51] In order to constrain the thermal evolution within middle and lower crust of the Famatina arc, we have combined modeled thermal profiles with the diffusive zoning of Fe and Mg in garnet within the Villarcan Gneiss. Compositional zoning profiles from garnet within melanosome of the Villarcan Gneiss display patterns that are indicative of diffusive zoning that arises as a consequence of cooling via Fe-Mg exchange within garnet grains in contact with biotite (Figure 16). Such zoning profiles can be modeled through analytical and numerical approaches to estimate the cooling history of a given sample [e.g., *Ehlers et al.*, 1994a, 1994b; *Florence and Spear*, 1995; *Ganguly and Tirone*, 1999; *Hauzenberger et al.*, 2005]. We have modeled the diffusive zoning of Fe and Mg in garnet of the Villarcan Gneiss using the program THERMAL HISTORY [*Robl et al.*, 2007]. The model assumes (1) garnet crystals can be approximated as spherical, (2) garnet is surrounded by biotite, (3) the amount of garnet to biotite is constant, (4) chemical equilibrium between the two minerals is achieved through binary exchange of Fe and Mg, and (5) diffusion in biotite is infinitely fast with respect to garnet. A modeled profile for a linear cooling history of 5°C/Ma is shown in Figure 15. The model reasonably matches the measured element concentration at the rim of garnet but somewhat overestimates the garnet core composition.

[52] In order to asses more realistic and complex thermal histories from peak granulite facies, we have modeled the cooling history as described by the thermal relaxation of an initial one-dimensional step-shaped temperature distribution [e.g., *Stüwe*, 1995] and combine the results with

regional age data and the above temperature dependent element distributions in garnet. The modeled temperature-time history is shown in Figure 16, and the details of the model are given in Appendix E. We model the thermal history for a partially melted heat source using a modified heat capacity that accounts for the effects of latent heat in partially molten rocks [*Stüwe*, 1995]. A modeled temperature-time history that assumes a constant value of latent heat fails to reproduce the observed zoning profile in garnet (Figure 15). In contrast, a model that incorporates the effects of latent heat not only reproduces the observed zoning profile at the garnet rim but also best fits the observed garnet core composition (Figure 16). Rather than assume accepted average closure temperatures for regional isotopic age data, the closure temperatures for multiple mineral phases and isotopic systems are calculated via the Dodson equation [*Dodson*, 1973] using the parameters listed in Appendix E, the reported mineral grain sizes, and the cooling rates calculated from the above thermal model (Figure 16) that accurately reproduces the observed diffusion profiles in garnet from the Villarcan Gneiss. The majority of high temperature ($\geq 500°C$) isotopic ages cluster between 420 and 450 Ma. A coarse grained (2–4 cm) garnet Sm-Nd age of 465 ± 5 Ma [*Galindo et al.*, 2004] likely records peak metamorphic conditions, while finer grained garnet samples record cooling ages for the Sm-Nd and Lu-Hf systems. The ages are consistent with the modeled cooling paths from peak metamorphism at ∼465 Ma through ∼420 Ma, after which cooling ages for multiple mineral phases and isotopic systems deviate substantially from the temperature-time paths, requiring increased cooling rates via exhumation.

[53] The results of the modeling suggest that the middle and lower crust of the Famatina arc remained partially molten for at least 20–30 Ma following Ordovician migmatization. Migmatization at peak temperatures occurred at ∼465 Ma, and garnet, titanite, and amphibole do not record cooling below the solidus (∼650°C) until ∼445–435 Ma. Regional cooling ages of amphibole, muscovite, and biotite deviate from the modeled cooling histories after ∼420 Ma and suggest more rapid cooling at that time.

5.3. Ordovician Melting and the Evolution of the Famatina Orogen

[54] Synconvergent extension is a well-recognized process in both active and ancient convergent margins [e.g., *Burchfiel and Royden*, 1985; *Wallis et al.*, 1993; *Wells et al.*, 2012]. Transitions from convergence to extension during an orogenic cycle result from the linked interaction between plate bounding forces, the thermal and rheologic evolution of the lithosphere, and contrasts in gravitational potential energy within an orogen [e.g., *England and Thompson*, 1986; *Dewey*, 1988]. Melting of the middle and lower crust is often associated with enhanced crustal weakening, and numerous studies have linked partial melting with strain localization [e.g., *Hollister and Crawford*, 1986; *Brown and Solar*, 1998]. In addition, the presence of partial melt and resulting buoyancy can drive extension and/or orogenic collapse [e.g., *Hollister*, 1993; *Brown and Dallmeyer*, 1996; *Vanderhaeghe and Teyssier*, 1997; *Teyssier and Whitney*, 2002]. Our results from this study combined with existing regional data, however, indicate that weakening and enhanced buoyancy of long-lived partial melt in the middle and lower crust of the Famatina orogen was not sufficient to drive extension or exhumation, thus requiring and alternative mechanism to trigger extension.

[55] The Famatina margin experienced Ordovician granulite facies migmatization of the middle and lower crust during terrane accretion. Figure 16b summarizes the regional igneous and metamorphic ages throughout the Famatina margin with respect to significant deformation episodes and tectonic events. Peak migmatization throughout the middle and lower crust of the Famatina margin was synchronous with regional convergence and initial collision of the Precordillera terrane. Zircon and monazite ages throughout the Famatina margin record peak granulite facies migmatization at ∼475–460 Ma [e.g., *Grissom et al.*, 1998; *Baldo et al.*, 2001; *Büttner et al.*, 2005; *Steenken et al.*, 2006; *Gallien et al.*, 2010; *Ducea et al.*, 2010; *Casquet et al.*, 2012]. This period coincides with voluminous magmatism in the Famatina arc (∼485–465 Ma) [*Ducea et al.*, 2010], initial collision of the Precordillera terrane (∼470 Ma) [*Fanning et al.*, 2004], retro-arc east-vergent thrusting (∼470 Ma) [*Astini and Davila*, 2004], and oblique top-to-the-west thrusting in the middle to lower crust [*Mulcahy et al.*, 2011].

[56] The modeled cooling history requires that melt was present in the middle and lower crust of the Famatina margin throughout continued convergence and collision. The cooling ages of garnet, titanite, and amphibole suggest that granulite facies migmatites cooled from peak temperatures to below the solidus (∼650°C for an average pelite composition in the system NCKFMASH) [*White et al.*, 2001] by ∼445–435 Ma. The convergence history recorded in top-to-the-west ductile shear zones of the Sierra de Pie de Palo [*Mulcahy et al.*, 2011] and regional stratigraphic evidence [*Astini et al.*, 1995; *Astini*, 1998; *Thomas and Astini*, 2007] suggest the final stages of Precordillera terrane collision and accretion occurred in the Late Ordovician (∼458-449 Ma).

[57] While the timing of melting and convergence were coeval, there is no evidence of extension or significant regional exhumation recorded during the time of widespread melting. Synconvergent extension on top-to-the-east shear zones is recorded in the Sierra de Pie de Palo at ∼436 Ma, following crystallization of middle and lower crustal migmatites. Continued extension and exhumation is recorded through ∼417 Ma as evidence by $^{40}Ar/^{39}Ar$ cooling ages across the Sierra de Pie de Palo [*Ramos et al.*, 1998; *Mulcahy et al.*, 2011].

[58] Throughout the time period of extensive cooling from peak granulite conditions and crystallization of regional migmatites, the middle and lower crust of the Famatina arc margin would have strengthened significantly [e.g., *Burg and Vigneresse*, 2002]. A thick crust of mafic material and/or partial eclogite underlying the western Sierra Pampeanas is supported by geophysical evidence [*Gilbert et al.*, 2006; *Alvarado et al.*, 2007; *Gans et al.*, 2011]. The presence of this thickened mafic crust implies that crustal delamination was not a driving factor of extension.

[59] The fact the regional migmatites would have crystallized prior the onset of extension and the lack of evidence for delamination requires an alternative mechanism of extension and exhumation. As discussed above, time period of ∼436 Ma coincides with the end of Precordillera terrane accretion outboard of the Famatina margin. Decreased

regional compressive stress associated with the end of collision may have facilitated the onset of regional extension at that time period.

5.4. Devonian Melting and Deformation

[60] In contrast to the protracted and regionally extensive Ordovician granulite facies metamorphism, melting, metamorphism, and exhumation of the Rio Las Chacras Formation occurred over a short time interval and was regionally localized. Our combined PT data, geochronology, and thermochronology indicate metamorphism and migmatization occurred at lower crustal conditions between ~411 and 403 Ma. This time period was contemporaneous with deformation east of the Valle Fertil lineament where strike-slip and transpressive shear zones have been documented between ~419 and 402 Ma [*von Gosen et al.*, 2002; *Hockenreiner et al.*, 2003; *Whitmeyer*, 2004; *Miller and Sollner*, 2005; *Steenken et al.*, 2010]. The localized and rapid burial, metamorphism, and exhumation of the Rio Las Chacras Formation and regional tectonic setting are consistent with models proposing the initiation of strike-slip deformation along the Valle Fertil lineament at that time period [*Roeske et al.*, 2008]. In addition, layered gabbros and mafic sills along the western margin of the Precordillera suggest that a new plate boundary was established by the Late Silurian (≥418 Ma) and was subsequently followed by collision of the Chilenia terrane in the Early to Middle Devonian (~385 Ma) [*Davis et al.*, 1999, 2000; *Willner et al.*, 2011].

6. Conclusions

[61] The Loma de Las Chacras preserves individual lithotectonic units that experienced distinct metamorphic, magmatic, and deformation histories. At the lowest structural levels, the kyanite-K-feldspar pelitic migmatites of the Villarcan Gneiss record a counterclockwise PT path that culminated in peak granulite facies metamorphism at ~12 kbar and ~868°C at ~465 Ma, followed by near isobaric cooling. In contrast, the Rio Las Chacras Formation did not experience the Ordovician granulite event. The unit underwent peak metamorphism at ~411–407 Ma, followed by rapid cooling, synchronous with exhumation of the Villarcan Gneiss. The two units were juxtaposed along the Rio Las Chacras-Villarcan shear zone and experienced a shared metamorphic history post ~407 Ma, when they were deformed and overprinted by the lower grade Don Juan–Flechal shear zone.

[62] Ordovician migmatization occurred relatively early in the orogenic cycle, synchronous with voluminous arc magmatism and magmatic underplating. Lower-crustal kyanite-bearing migmatites west of the Valle Fertil lineament in Las Chacras and middle-crustal sillimanite bearing counterparts to the east remained at temperatures above the solidus for ~20–30 Ma following peak granulite facies metamorphism, during a period marked by regional oblique convergence and collision of the Precordillera terrane. Synconvergent extension occurred after regional migmatites cooled beneath their solidus and was synchronous with the end of Precordillera terrane accretion at ~436 Ma. A second, local phase of Devonian melting within the high-pressure amphibolite facies Rio Las Chacras Formation, however, does appear to have been associated with localized extension and exhumation. Geochronology from multiple isotopic systems require rapid burial and exhumation of the Rio Las Chacras Formation at a time scale that is mostly consistent with localized deformation within a strike-slip zone. The timing of melting and deformation is synchronous with the onset of regional strike-slip deformation related convergence and accretion of the Chilenia terrane. The regional deformation, metamorphic, and magmatic histories imply that Ordovician middle and lower crustal migmatization did not result in exhumation and extension within the Famatina margin. Instead, the onset of synconvergent extension and continued exhumation was synchronous with the establishment of new plate margin and successive terrane accretion, consistent with a change in plate boundary forces as the driving mechanism of extension.

Appendix A: Mineral Compositions

[63] Mineral compositions determined by electron microprobe and used in the thermobarometry calculations and for dating by various isotopic systems are provided in the following tables:

Table A1. Representative garnet compositions from the Rio Las Chacras Formation
Table A2. Representative garnet compositions from the Villarcan Gneiss
Table A3. Representative biotite compositions from the Rio Las Chacras Formation
Table A4. Representative biotite compositions from the Villarcan Gneiss
Table A5. Representative feldspar compositions from the Rio Las Chacras Formation
Table A6. Representative feldspar compositions from the Villarcan Gneiss
Table A7. Representative amphibole compositions from the Rio Las Chacras Formation
Table A8. Representative amphibole compositions from the Villarcan Gneiss
Table A9. Representative epidote/clinozoisite compositions
Table A10. Representative staurolite and gahnite compositions from the schist of Rio Las Chacras Formation
Table A11. Representative titanite compositions

Appendix B: U-Pb Geochronology

[64] All analyses were performed on the SHRIMP-RG ion microprobe at the United States Geological Survey-Stanford Microanalytical Center at Stanford University. The analytical routine followed *Williams* [1998]. Data reduction utilized the SQUID program of *Ludwig* [2003]. Data are provided in the following tables:

Table B1. U-Pb zircon geochronologic data
Table B2. U-Pb titanite geochronologic data

Appendix C: Lu-Hf Geochronology

[65] Data are provided in the following table.

Table C1. Lu-Hf isotopic data for garnet geochronology.

Appendix D: $^{40}Ar/^{39}Ar$ Geochronology

[66] All analyses were performed at the Berkeley Geochronology Center. $^{40}Ar/^{39}Ar$ ages were calculated following the calibration of *Renne et al.* [2010].

Table D1. Isotopic data for $^{40}Ar/^{39}Ar$ geochronology.

Appendix E: Thermal Modeling

[67] Cooling of Ordovician migmatites from peak granulite conditions within the Famatina arc was modeled by the thermal relaxation of an initial one-dimensional step-shaped temperature distribution using the following explicit finite difference element scheme as described by *Stüwe* [1995]:

$$T_n^+ = T_n^- + \left(\frac{k\Delta t}{\rho c_{\mathrm{mod}}\Delta x^2}\right) + \left(T_{n+1}^- - 2T_n^- + T_{n-1}^-\right)$$

where T is temperature (K), k is thermal conductivity (J s^{-1} m^{-1} K^{-1}), t is the time, ρ is density (kg m^3), and c_{mod} is the modified heat capacity (J kg^{-1} K^{-1}) that is defined in the temperature region of the melting interval ($T_L > Tn > T_s$, where T_L is the liquidus temperature and T_S is the solidus temperature) as $c_{\mathrm{mod}} = c_p + LAe^{\alpha T^-_n}$ where c_p is the heat capacity (J kg^{-1} K^{-1}), L is the latent heat of fusion (kJ kg^{-1}), α is a parameter that describes the melt volume production with change in temperature, and A is constant defined as

$$A = \frac{\alpha}{e^{(\alpha T_L)} - e^{(\alpha T_S)}}$$

[68] Modeled temperature-time and cooling-rate evolutions were combined with equations of closure-temperature of a cooling system [e.g., *Dodson*, 1973] to calculate model closure temperatures from reported ages and mineral grain sizes in the literature. Model parameters and regional isotopic data plotted in Figure 16 are provided in the following tables:

Table E1. Model parameters for the Famatina arc.
Table E2. Regional isotopic data and calculated closure temperatures in Figure 16a.

[69] The histograms and density plots in Figure 16b were constructed from ages reported in the following references: *Sims et al.* [1998], *Pankhurst et al.* [1998], *Pankhurst and Rapela* [1998], *Grissom et al.* [1998], *Stuart-Smith et al.* [1999], *Rapela et al.* [2001], *Baldo et al.* [2001], *von Gosen et al.* [2002], *Hockenreiner et al.* [2003], *Lucassen and Becchio* [2003], *Porcher et al.* [2004], *Galindo et al.* [2004], *Büttner et al.* [2005], *Steenken et al.* [2006], *Mulcahy et al.* [2007], *Dahlquist et al.* [2008], *Castro de Machuca et al.* [2008], *Steenken et al.* [2008], *Morata et al.* [2010], *Ducea et al.* [2010], *Gallien et al.* [2010], *Chernicoff et al.* [2010], *Mulcahy et al.* [2011], and *Varela et al.* [2011].

[70] **Acknowledgments.** We would like to thank the citizens of Loma de Las Chacras for their hospitality during our field work. S.R. Mulcahy sincerely thanks Joseph Cain IV, Yamilla Gato, and Jose Mescua for their assistance in the field. We thank Michael Williams and an anonymous reviewer for thoughtful and critical reviews and Todd Ehlers and Lindsay Schoenbohm for their editorial handling of the manuscript.

References

Alvarado, P., S. Beck, and G. Zandt (2007), Crustal structure of the south-central Andes Cordillera and backarc region from regional waveform modelling, *Geophys. J. Int.*, *170*, 858–875.

Astini, R. (1998), Stratigraphical evidence supporting the rifting, drifting and collision of the Laurentian Precordillera terrane of western Argentina, *Geol. Soc. London Spec. Publ.*, *142*, 11–33.

Astini, R. A., and F. M. Davila (2004), Ordovician back arc foreland and Ocloyic thrust belt development on the western Gondwana margin as a response to Precordillera terrane accretion, *Tectonics*, *23*, TC4008, doi:10.1029/2003TC001620.

Astini, R. A., J. L. Benedetto, and N. E. Vaccari (1995), The Early Paleozoic evolution of the Argentine Precordillera as a Laurentian rifted, drifted, and collided terrane: A geodynamic model, *Geol. Soc. Am. Bull.*, *107*(3), 253–273.

Baldo, E., C. Casquet, C. W. Rapela, R. J. Pankhurst, C. Galindo, C. M. Fanning, and J. Saavedra (2001), Ordovician metamorphism at the south-western margin of Gondwana: P-T conditions and U-Pb SHRIMP ages from the Loma de Las Chacras, Sierras Pampeanas, *Proc. III South Am. Sym. of Isotope Geol.*, *3*, 544–547.

Bouvier, A., J. D. Vervoort, and P. J. Patchett (2008), The Lu-Hf and Sm Nd isotopic composition of CHUR: Constraints from unequilibrated chondrites and implications for the bulk composition of terrestrial planets, *Earth Planet. Sci. Lett.*, *273*, 48–57, doi:10.1016/j.epsl.2008.06.010.

Brown, M., and R. D. Dallmeyer (1996), Rapid Variscan exhumation and role of magma in core complex formation: Southern Brittany metamorphic belt, France, *J. Metamorph. Geol.*, *14*, 361–379.

Brown, M., and G. S. Solar (1998), Shear-zone systems and melts: Feedback relations and self-organization in orogenic belts, *J. Struct. Geol.*, *20*, 211–227.

Burchfiel, B. C., and L. H. Royden (1985), North-South extension within the convergent Himalaya region, *Geology*, *13*, 679–682, doi:10.1130/0091-7613(1985)13<679:NEWTCH>2.0.CO;2.

Burg, J. P., and J. L. Vigneresse (2002), Non-linear feedback loops in the rheology of cooling-crystallizing felsic magma and heating-melting felsic rock, *Geol. Soc. London Spec. Publ.*, *200*(1), 275–292, doi:10.1144/GSL.SP.2001.200.01.16.

Büttner, S. H., J. Glodny, F. Lucassen, K. Wemmer, S. Erdmann, R. Handler, and G. Franz (2005), Ordovician metamorphism and plutonism in the Sierra de Quilmes metamorphic complex: Implications for the tectonic setting of the northern Sierras Pampeanas (NW Argentina), *Lithos*, *83*(1-2), 143–181, doi:10.1016/j.lithos.2005.01.006.

Cain, J. C., IV (2006), Characterization of the Don Juan Shear Zone: Devonian extension in the Western Sierra Pampeanas Provincia, San Juan, Argentina, M. S. Thesis, University of California, Davis.

Casquet, C., C. W. Rapela, R. J. Pankhurst, E. Baldo, C. Galindo, C. M. Fanning, and J. Dahlquist (2012), Fast sediment underplating and essentially coeval juvenile magmatism in the Ordovician margin of Gondwana, Western Sierras Pampeanas, Argentina, *Gondwana Res.*, *22*, 664–673, doi:10.1016/j.gr.2012.05.001.

Castro de Machuca, B., G. Arancibia, D. Morata, M. Belmar, L. Previley, and S. Pontoriero (2008), Pt evolution of an Early Silurian medium-grade shear zone on the west side of the Famatinian magmatic arc, Argentina: Implications for the assembly of the Western Gondwana margin, *Gondwana Res.*, *13*, 216–226, doi:10.1016/j.gr.2007.05.005.

Cherniak, D. (1993), Lead diffusion in titanite and preliminary results on the effects of radiation damage on Pb transport, *Chem. Geol.*, *110*(1-3), 177–194, doi:10.1016/0009-2541(93)90253-F.

Chernicoff, C. J., E. O. Zappettini, J. a. O. Santos, S. Allchurch, and N. J. McNaughton (2010), The southern segment of the Famatinian magmatic arc, La Pampa Province, Argentina, *Gondwana Res.*, *17*(4), 662–675, doi:10.1016/j.gr.2009.10.008.

Dahlquist, J. A., R. R. Pankhurst, W. Carlos, C. Galindo, P. Alasino, C. Fanning, J. Saavedra, and E. Baldo (2008), New SHRIMP u-Pb data from the Famatina complex: Constraining early-mid Ordovician Famatinian magmatism in the Sierras Pampeanas, Argentina, *Geol. Acta*, *6*(4), 319–333.

Davis, J., S. Roeske, W. McClelland, and L. Snee (1999), Closing the ocean between the Precordillera terrane and Chilenia: Early Devonian ophiolite emplacement and deformation in the southwest Precordillera, *Geol. Soc. Am. Special Paper*, *336*, 115–138.

Davis, J. S., S. M. Roeske, W. C. McClelland, and S. M. Kay (2000), Mafic and ultramafic crustal fragments of the southwestern Precordillera terrane and their bearing on tectonic models of the early Paleozoic in western Argentina, *Geology*, *28*(2), 171–174, doi:10.1130/0091-7613(2000)28.

Delpino, S. H., E. A. Bjerg, G. R. Ferracutti, and A. Mogessie (2007), Counterclockwise tectonometamorphic evolution of the Pringles Metamorphic Complex, Sierras Pampeanas of San Luis (Argentina), *J. South Amer. Earth Sci.*, *23*, 147–175, doi:10.1016/j.jsames.2006.09.019.

Dewey, J. F. (1988), Extension and collapse of orogens, *Tectonics*, *7*(6), 1123–1139, doi:10.1029/TC007i006p01123.

Dodson, M. H. (1973), Closure temperature in cooling geochronological and petrological systems, *Contrib. Mineral. Petrol.*, *40*(3), 259–274, doi:10.1007/BF00373790.

Ducea, M. N., J. E. Otamendi, G. Bergantz, K. M. Stair, V. A. Valencia, and G. E. Gehrels (2010), Timing constraints on building an intermediate plutonic arc crustal section: U-Pb zircon geochronology of the Sierra Valle Fertil–La Huerta, Famatinian arc, Argentina, *Tectonics*, *29*, TC4002, doi:10.1029/2009TC002615.

Ehlers, K., R. Powell, and K. Stuwe (1994a), Cooling rate histories from garnet + biotite equilibrium, *Am. Mineral.*, *79*(7-8), 737–744.

Ehlers, K., K. Stüwe, R. Powell, M. Sandiford, and W. Frank (1994b), Thermometrically inferred cooling rates from the Plattengneis, Koralm region, Eastern Alps, *Earth Planet. Sci. Lett.*, *125*(1-4), 307–321, doi:10.1016/0012-821X(94)90223-2.

England, P. C., and A. B. Thompson (1986), Some thermal and tectonic models for crustal melting in continental collision zones, *Collision Tectonics, Special Publication Geol. Soc. London*, *19*, 83–94.

Ernst, W. G., and J. Liou (1998), Experimental phase-equilibrium study of Al- and Ti-contents of calcic amphibole in MORB—A semiquantitative thermobarometer, *Am. Mineral.*, *83*, 952–969.

Fanning, C. M., R. J. Pankhurst, C. W. Rapela, E. G. Baldo, C. Casquet, and C. Galindo (2004), K-bentonites in the Argentine Precordillera contemporaneous with rhyolite volcanism in the Famatinian Arc, *J. Geol. Soc.*, *161*, 747–756.

Florence, F. P., and F. S. Spear (1995), Intergranular diffusion kinetics of Fe and Mg during retrograde metamorphism of a pelitic gneiss from the Adirondack Mountains, *Earth Planet. Sci. Lett.*, *134*(3-4), 329–340, doi:10.1016/0012-821X(95)00129-Z.

Galindo, C., J. Murra, E. Baldo, C. Casquet, C. W. Rapela, R. J. Pankhurst, and J. Dahlquist (2004), Datacion Sm-Nd metamorfismo en la Sierra de las Imanas (Sierras Pampeanas Occidentales, Argentina), *Geogaceta*, *35*, 75–78.

Gallien, F., A. Mogessie, E. Bjerg, S. Delpino, B. de Machuca, M. Thoni, and U. Klotzli (2010), Timing and rate of granulite facies metamorphism and cooling from multi-mineral chronology on migmatitic gneisses, Sierras de La Huerta and Valle Fértil, NW Argentina, *Lithos*, *114*, 229–252.

Ganguly, J., and M. Tirone (1999), Diffusion closure temperature and age of a mineral with arbitrary extent of diffusion: Theoretical formulation and applications, *Earth Planet. Sci. Lett.*, *170*, 131–140.

Gans, C. R., S. L. Beck, G. Zandt, H. Gilbert, P. Alvarado, M. Anderson, and L. Linkimer (2011), Continental and oceanic crustal structure of the Pampean flat slab region, western Argentina, using receiver function analysis: New high-resolution results, *Geophys. J. Int.*, *186*, 45–58.

Gilbert, H., S. Beck, and G. Zandt (2006), Lithospheric and upper mantle structure of central Chile and Argentina, *Geophys. J. Int.*, *165*(1), 383–398.

Grissom, G. C., S. M. Debari, and L. W. Snee (1998), Geology of the Sierra de Fiambala, Northwest Argentina: Implications for Early Paleozoic Andean tectonics, in *The Proto-Andean Margin of Gondwana,* vol. 142, edited by R. J. Pankhurst and C. W. Rapela, pp. 297–324, Geological Society Special Publication, London.

Hauzenberger, C. A., A. Mogessie, G. Hoinkes, A. Felfernig, E. A. Bjerg, J. Kostadinoff, S. Delpino, and L. Dimieri (2001), Metamorphic evolution of the Sierras de San Luis, Argentina: Granulite facies metamorphism related to mafic intrusions, *Mineral. Petrol.*, *71*, 95–126.

Hauzenberger, C. A., J. Robl, and K. Stüwe (2005), Garnet zoning in high pressure granulite-facies metapelites, Mozambique belt, SE-Kenya: Constraints on the cooling history, *Eur. J. Mineral.*, *17*, 43–55, doi:10.1127/0935-1221/2005/0017-0043.

Hockenreiner, M., F. Sollner, and H. Miller (2003), Dating the TIPA shear zone: An Early Devonian terrane boundary between the Famatinan and Pampean systems (NW Argentina), *J. South Amer. Earth Sci.*, *16*, 45–66.

Holland, T., and J. Blundy (1994), Non-ideal interactions in calcic amphiboles and their bearing on amphibole-plagioclase thermobarometry, *Contrib. Mineral. Petrol.*, *116*(4), 433–447, doi:10.1007/BF00310910.

Hollister, L. S., and M. L. Crawford (1986), Melt-enhanced deformation: A major tectonic process, *Geology*, *14*, 558–561.

Hollister, L. S. (1993), The role of melt in the uplift and exhumation of orogenic belts, *Chem. Geol.*, *108*, 31–48.

Kretz, R. (1983), Symbols for rock-forming minerals, *Am. J. Sci.*, *68*, 277–279.

Larrovere, M. A., C. R. de los Hoyos, A. J. Toselli, J. N. Rossi, M. A. Basei, and M. E. Belmar (2011), High T/P evolution and metamorphic ages of the migmatitic basement of Northern Sierras Pampeanas, Argentina: Characterization of a mid-crustal segment of the Famatinian belt, *J. South Amer. Earth Sci.*, *31*, 279–297, doi:10.1016/j.jsames.2010.11.006.

Lucassen, F., and R. Becchio (2003), Timing of high-grade metamorphism: Early Palaeozoic U–Pb formation ages of titanite indicate long-standing high-T conditions at the western margin of Gondwana (Argentina, 26-29C), *J. Metamorph. Geol.*, *21*, 649–662.

Ludwig, K. R. (1998), On the treatment of concordant uranium-lead ages—Evidence for an early Proterozoic mantle plume beneath rifted Archean continental lithosphere, *Geochim. Cosmochim. Acta*, *62*(4), 665–676.

Ludwig, K. R. (2003), *Users Manual for ISOPLOT 3.00: A Geochronological Toolkit for Microsoft Excel*, Berkeley Geochronology Center Special Publication, Berkeley, CA.

Miller, H., and F. Sollner (2005), The Famatina complex (NW Argentina): Back-docking of an island arc or terrane accretion? Early Palaeozoic geodynamics at the western Gondwana margin, in *Terrane Processes at the Margins of Gondwana,* vol.246, edited by A. M. P. Vaughan, P. T. Leat, and R. J. Pankhurst, pp. 241–256, Geological Society Special Publications, London.

Morata, D., B. Castro de Machuca, G. Arancibia, S. Pontoriero, and C. M. Fanning (2010), Peraluminous Grenvillian TTG in the Sierra de Pie de Palo, Western Sierras Pampeanas, Argentina: Petrology, geochronology, geochemistry and petrogenetic implications, *Precambrian Res.*, *177*, 308–322, doi:10.1016/j.precamres.2010.01.001.

Mulcahy, S. R., S. M. Roeske, W. C. McClelland, S. Nomade, and P. R. Renne (2007), Cambrian initiation of the Las Pirquitas thrust of the western Sierras Pampeanas, Argentina: Implications for the tectonic evolution of the proto-Andean margin of South America, *Geology*, *35*, 443–446, doi:10.1130/G23436A.1.

Mulcahy, S. R., S. M. Roeske, W. C. McClelland, F. Jourdan, A. Iriondo, P. R. Renne, J. D. Vervoort, and G. I. Vujovich (2011), Structural evolution of a composite middle to lower crustal section: The Sierra de Pie de Palo, northwest Argentina, *Tectonics*, *30*, TC1005, doi:10.1029/2009TC002656.

Murra, J. A., and E. G. Baldo (2006), Evolución tectonotermal ordovícica del borde occidental del arco magmático Famatiniano: Metamorfismo de las rocas máficas y ultramáficas de la Sierra de la Huerta de Las Imanas (Sierras Pampeanas, Argentina), *Rev. Geol. Chile*, *33*, 277–298, doi:10.4067/S0716-02082006000200004.

Otamendi, J., A. Tibaldi, G. Vujovich, and G. Viñao (2008), Metamorphic evolution of migmatites from the deep Famatinian arc crust exposed in Sierras Valle Fertil-La Huerta, San Juan, Argentina, *J. South Amer. Earth Sci.*, *25*, 313–335.

Otamendi, J. E., M. N. Ducea, and G. W. Bergantz (2012), Geological, Petrological and Geochemical Evidence for Progressive Construction of an Arc Crustal Section, Sierra de Valle Fertil, Famatinian Arc, Argentina, *J. Petrol.*, *53*(4), 761–800, doi:10.1093/petrology/egr079.

Pankhurst, R., and C. Rapela (1998), The proto-Andean margin of Gondwana: An introduction, in *The Proto-Andean Margin of Gondwan,* vol. 142, edited by R. J. Pankhurst and C. W. Rapela, pp. 1–9, Geological Society Special Publications, London.

Pankhurst, R. J., C. W. Rapela, J. Saavedra, E. Baldo, J. Dahlquist, I. Pascua, and C. M. Fanning (1998), The Famatinian magmatic arc in the central Sierras Pampeanas: An Early to Mid-Ordovician continental arc on the Gondwana margin, in *The Proto-Andean Margin of Gondwan,* vol. 142, edited by R. J. Pankhurst and C. W. Rapela, pp. 343–367, Geological Society Special Publications, London.

Pankhurst, R. J., C. W. Rapela, and C. M. Fanning (2000), Age and origin of coeval TTG, I- and S-type granites in the Famatinian belt of NW Argentina, *Trans. R. Soc. Edinburgh: Earth Sci.*, *91*, 151–168.

Porcher, C. C., L. A. D. Fernandes, G. I. Vujovich, and C. J. Chernicoff (2004), Thermobarometry, Sm/Nd ages and geophysical evidence for the location of the suture zone between Cuyania and western proto-Andean margin of Gondwana, *Gondwana Res.*, *7*, 1057–1076.

Powell, R., and T. Holland (1994), Optimal geothermometry and geobarometry, *Am. Mineral.*, *79*, 120–133.

Quenardelle, S., and V. Ramos (1999), Ordovician western Sierras Pampeanas magmatic belt: Record of Precordillera accretionin Argentina, in *Laurentia-Gondwana Connections before Pangea,* vol. 336, edited by V. A. Ramos and J. D. Keppie, pp. 63–86, Geological Society of America Special Papers, Boulder, Colo.

Ramos, V. A., R. D. Dallmeyer, and G. Vujovich (1998), Time constraints on the Early Paleozoic docking of the Precordillera, central Argentina, vol. 142, in *The Proto-Andean Margin of Gondwana*, edited by R. J. Pankhurst and C. W. Rapela, pp. 143–158, Geological Society Special Publication, London.

Rapela, C., R. Pankhurst, E. Baldo, C. Casquet, C. Galindo, C. Fanning, and J. Saavedra (2001), Ordovician metamorphism in the Sierras Pampeanas: New U-Pb shrimp ages in Central-East Valle Fértil and the Velasco Batholith, paper present at III South American Symposium on Isotope Geology, Extended Abstract Volume (CD), Sociedad Geológica de Chile, Santiago, Chile.

Renne, P. R., R. Mundil, G. Balco, K. Min, and K. R. Ludwig (2010), Joint determination of 40K decay constants and 40Ar*/40K for the Fish Canyon sanidine standard, and improved accuracy for 40Ar/39Ar geochronology, *Geochim. Cosmochim. Acta*, *74*, 5349–5367.

Robl, J., S. Hergarten, K. Stüwe, and C. Hauzenberger (2007), THERMAL HISTORY: A new software to interpret diffusive zoning profiles in garnet, *Comput. Geosci.*, *33*, 760–772.

Roeske, S., S. R. Mulcahy, W. McClelland, and J. Cain (2008), Characteristics of middle and deep crustal expression of an arc-forearc boundary strike-slip fault system, Abstract T43E-06 presented at 2008 Fall Meeting, AGU, Washington, D. C.

Scherer, E. E., K. L. Cameron, and J. Blichert-Toft (2000), Lu-Hf garnet geochronology: Closure temperature realtive to the Sm-Nd system and the effects of trace mineral inclusions, *Geochim. Cosmochim. Acta*, *64*(19), 3413–3432.

Sims, J. P., T. R. Ireland, A. Camacho, P. Lyons, P. E. Pieters, R. G. Skirrow, P. G. Stuart-Smith, and R. Miro (1998), U-Pb, Th-Pb and Ar-Ar geochronology from the Southern Sierras Pampeanas, Argentina: Implications for the Palaeozoic tectonic evolution of the Western Gondwana margin, in *The Proto-Andean Margin of Gondwana,* vol. 142, edited by R. J. Pankhurst and C. W. Rapela, pp. 259–281, Geological Society Special Publications, London.

Soderlund, U., P. Patchett, J. Vervoort, and C. Isachsen (2004), The 176Lu decay constant determined by Lu-Hf and U-Pb isotope systematics of Precambrian mafic intrusions, *Earth Planet. Sci. Lett.*, *219*, 311–324.

Spear, F. S., M. J. Kohn, and J. T. Cheney (1999), P-T paths from anatectic pelites, *Contrib. Mineral. Petrol.*, *134*, 17–32.

Steenken, A., S. Siegesmund, M. G. de Luchi, R. Frei, and K. Wemmer (2006), Neoproterozoic to Early Palaeozoic events in the Sierra de San Luis: Implications for the Famatinian geodynamics in the Eastern Sierras Pampeanas (Argentina), *J. Geol. Soc.*, *163*, 965–982.

Steenken, A., S. Siegesmund, K. Wemmer, and M. G. de Luchi (2008), Time constraints on the Famatinian and Achalian structural evolution of the basement of the Sierra de San Luis (Eastern Sierras Pampeanas, Argentina), *J. South Amer. Earth Sci.*, *25*, 336–358.

Steenken, A., M. G. de Luchi, C. Martínez Dopico, M. Drobe, K. Wemmer, and S. Siegesmund (2010), The Neoproterozoic-early Paleozoic metamorphic and magmatic evolution of the Eastern Sierras Pampeanas: An overview, *Int. J. Earth Sci.*, 1–24.

Stuart-Smith, P., A. Camacho, J. P. Sims, R. G. Skirrow, P. Lyons, P. E. Pieters, L. P. Black, and R. Miró (1999), Uranium-lead dating of felsic magmatic cycles in the southern Sierras Pampeanas, Argentina: Implications for the tectonic development of the proto-Andean Gondwana margin, in *Laurentia-Gondwana Connections Before Pangea,* vol. 336, edited by V. A. Ramos and J. D. Keppie, pp. 87–114, Geological Society of America Special Paper, Boulder, Colo.

Stüwe, K. (1995), Thermal buffering effects at the solidus. Implications for the equilibration of partially melted metamorphic rocks, *Tectonophysics*, *248*(1-2), 39–51, doi:10.1016/0040-1951(94)00282-E.

Teyssier, C., and D. L. Whitney (2002), Gneiss domes and orogeny, *Geology*, *30*, 1139–1142.

Thomas, W. A., and R. A. Astini (2007), Vestiges of an Ordovician west-vergent thin-skinned Ocloyic thrust belt in the Argentine Precordillera, Southern Central Andes, *J. Struct. Geol.*, 1–17.

Tibaldi, A. M., A. M. Alvarez-Valero, J. E. Otamendi, and E. A. Cristofollini (2011), Formation of paired pelitic and gabbroic migmatites: An empirical investigation of the consistency of geothermometers, geobarometers, and pseudosections, *Lithos*, *122*, 57–75.

Tibaldi, A. M., J. E. Otamendi, E. A. Cristofolini, I. Baliani, B. A. Walker, and G. W. Bergantz (2013), Reconstruction of the Early Ordovician Famatinian arc through thermobarometry in lower and middle crustal exposures, Sierra de Valle Fértil, Argentina, *Tectonophysics*, *589*, 151–166, doi:10.1016/j.tecto.2012.12.032.

Vanderhaeghe, O., and C. Teyssier (1997), Formation of the Shuswap metamorphic core complex during late-orogenic collapse of the Canadian Cordillera: Role of ductile thinning and partial melting of the mid- to lower crust, *Geodin. Acta*, *10*, 41–58.

Varela, R., M. A. S. Basei, P. D. Gonzalez, A. M. Sato, M. Naipauer, M. C. Neto, C. A. Cingolani, and V. T. Meira (2011), Accretion of Grenvillian terranes to the southwestern border of the Rio de la Plata craton, western Argentina, *Int. J. Earth Sci.*, *100*, 243–272.

von Gosen, W., W. Loske, and C. Prozzi (2002), New isotopic dating of intrusive rocks in the Sierra de San Luis (Argentina): Implications for the geodynamic history of the eastern Sierras Pampeanas, *J. South Amer. Earth Sci.*, *15*, 237–250.

Vujovich, G. I. (1994), Geología del basamento ígneo-metamórfico de la loma de Las Chacras, Sierra de La Huerta, San Juan, *Revista de La Asociación Geológica Argentina*, *49*, 321–336.

Wallis, S. R., J. P. Platt, and S. D. Knott (1993), Recognition of synconvergent extension in accretionary wedges with examples from the Calabrian Arc and eastern Alps, *Am. J. Sci.*, *293*, 463–494.

Wells, M. L., T. D. Hoisch, A. M. Cruz-Uribe, and J. D. Vervoort (2012), Geodynamics of synconvergent extension and tectonic mode switching: Constraints from the Sevier-Laramide orogen, *Tectonics*, *31*, TC1002, doi:10.1029/2011T002913.

White, R. W., R. Powell, and T. Holland (2001), Calculation of partial melting equilibria in the system Na2O-CaO-K2O-FeO-MgO-Al2O3-SiO2-H2O (NCKFMASH), *J. Metamorph. Geol.*, *19*, 139–154.

Whitmeyer, S. J. (2004), Regional deformation of the Sierra de San Luis, Argentina: Implications for the Paleozoic development of western Gondwana, *Tectonics*, *23*, TC1005, doi:10.1029/2003TC001542.

Williams, I. S. (1998), U-Th-Pb geochronology by ion microprobe, in *Applications of Microanalytical Techniques to Understanding Mineralizing Processes,* vol. 7, edited by M. A. McKibben, W. C. P. Shanks, and W. I. Ridley, 1–35, Reviews in Economic Geology, Society of Economic Geologists, Littleton, Colo.

Willner, A., A. Gerdes, H.-J. Massonne, A. Schmidt, M. Sudo, S. Thomson, and G. Vujovich (2011), The geodynamics of collision of a microplate (Chilenia) in Devonian times deduced by the pressure–temperature–time evolution within part of a collisional belt (Guarguaraz Complex, W-Argentina), *Contrib. Mineral. Petrol.*, *162*, 303–327.